

Nanoscale

Accepted Manuscript



This is an *Accepted Manuscript*, which has been through the Royal Society of Chemistry peer review process and has been accepted for publication.

Accepted Manuscripts are published online shortly after acceptance, before technical editing, formatting and proof reading. Using this free service, authors can make their results available to the community, in citable form, before we publish the edited article. We will replace this *Accepted Manuscript* with the edited and formatted *Advance Article* as soon as it is available.

You can find more information about *Accepted Manuscripts* in the [Information for Authors](#).

Please note that technical editing may introduce minor changes to the text and/or graphics, which may alter content. The journal's standard [Terms & Conditions](#) and the [Ethical guidelines](#) still apply. In no event shall the Royal Society of Chemistry be held responsible for any errors or omissions in this *Accepted Manuscript* or any consequences arising from the use of any information it contains.

ARTICLE

Building Up Strain in Colloidal Metal Nanoparticle Catalysts

Cite this: DOI: 10.1039/x0xx00000x

Brian T. Sneed,^a Allison P. Young,^a and Chia-Kuang Tsung^{a,*}Received 00th January 2012,
Accepted 00th January 2012

DOI: 10.1039/x0xx00000x

www.rsc.org/

The focus on surface lattice strain in nanostructures as a fundamental research topic has gained momentum in recent years as scientists investigated its significant impact on the surface electronic structure and catalytic properties of nanomaterials. Researchers have begun to tell a more complete story of catalysis from a perspective which brings this concept to the forefront of the discussion. The nano-‘realm’ makes the effects of surface lattice strain, which acts on the same spatial scales, more pronounced due to a higher ratio of surface to bulk atoms. This is especially evident in the field of metal nanoparticle catalysis, where displacement of atoms on surfaces can significantly alter the sorption properties of molecules. In part, the concept of strain-engineering for catalysis opened up due to the achievements that were made in the synthesis of a more sophisticated nanoparticle library from an ever-expanding set of methodologies. Developing synthesis methods for metal nanoparticles with well-defined and strained architectures is a worthy goal that, if reached, will have considerable impact in the search for catalysts. In this review, we summarize the recent accomplishments in the area of surface lattice-strained metal nanoparticle synthesis, framing the discussion from the important perspective of surface lattice strain effects in catalysis.

Introduction

Lattice strain has been an important research topic in materials science for many decades,¹ and this continues due to the growth of the field of nanoscience and technology.^{2,3} Many important discoveries have been made regarding the prevalent nature of lattice strain in recent years, dealing primarily with its effects on the reactivity of metal nanocrystal electrocatalysts.^{2,4-23} Surface lattice strain is an important factor to be considered and controlled in tuning catalytic performance of nanocrystals, as its impact can be felt at the surface, even with the source of strain being buried several atomic layers deep in a nanostructure. This demands a new paradigm for studies of structure and catalysis at the nanoscale, one that could offer a much more complete mechanistic understanding of the catalyst/molecule surface interaction; albeit with the added complexity of introducing yet another optimization parameter to the list, which already includes the factors of size, shape, composition, choice of support, and catalytic environment. Improved catalysis for energy storage and conversion will be tied to the future development of this field for more sustainable and zero-emission technologies.²⁴

By carefully engineering the degree of surface lattice strain in a metal nanoparticle, the sorption energies of molecules can be optimized for a particular chemical reaction.^{4,10,25-28} This can be explained by a change in the surface d-band center of a metal nanoparticle due to lattice distortion.^{5,6,9-11,25,29-31} The changes depend on the transition metal element in question; however, in general, expansive strain causes a reduction in orbital overlap, narrowing the d-band and raising the d-band

center, whereas compressive strain increases orbital overlap, widening the d-band and lowering the d-band center.³² The altered d-band affects the molecular sorption energies, in turn, contributing to the catalytic behavior. The classical Sabatier principle³³ follows for strain effects.^{34,35} The optimum rate of reaction is achieved by balancing the sorption strength so that molecules bind well enough to react quickly, but also desorb fast enough to regenerate active surface sites. The direction and degree of strain-tuning of surfaces that needs to take place to enhance performance are dependent on the specific reaction and metal catalysts in question. For example, Pt-based oxygen reduction catalysis is improved by weakening the binding of adsorbed oxygen intermediates through a downward d-band shift and broadening caused by compressive strain,¹⁰ whereas expansive strain of Pd-based catalyst surfaces likely improves formic acid oxidation electrocatalysis through weakening of the binding of adsorbed CO intermediates.^{16,20}

Since subtle shifts in surface lattice arrangements can have considerable impacts to catalytic behavior via this mechanism, the development of the synthesis of metal nanoparticles with a high degree of control of lattice strain is important for future research. Several types of metal nanoparticles with strained surfaces can be generated by a variety of methods. A comprehensive review has been published in 2012 and we will focus on the new developments in this field.² This review will first describe the different sources of strain in late transition metal nanoparticles, highlighting the synthesis of the differently strained basic architectures. This builds in complexity to the discussion of recently designed, more sophisticated strained archetypes. The advancements in catalysis by these structures

and their characterization are then discussed. Finally, several of the challenges facing the synthesis and catalysis by strained metal nanoparticle architectures are described, and a perspective on the focus of future research endeavors is given.

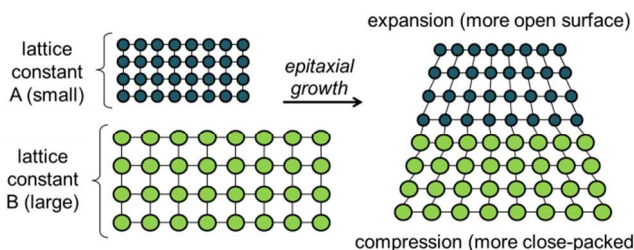


Figure 1. Illustration of strain for epitaxial films (core-shell nanoparticle structure).

Lattice-Strained Metal Nanoparticle Archetypes

As generally defined, lattice strain is a measure of the deformation (or distortion) of a lattice caused by stress (tension) at the interface between phases which displaces atoms in the lattice, resulting in compression or expansion away from the ideal bulk lattice parameters (Figure 1). The effects of strain propagate through the crystal, but decay further away from the source due to relaxation around the interface. This can have an impact on the properties of the metal surface, providing the source of strain is within a few nanometers of the surface structure. Lattice strain in nanoparticles is generated by a variety of sources and can be tuned by an assortment of properties: by particle size, shape, twinning, by the lattice mismatch between metals in multimetallic core-shell nanoparticle structures, and by alloying (Figure 2). It is important to note that multiple sources of strain are operating simultaneously in most multimetallic nanoparticles and sometimes it is challenging to decouple the ligand and ensemble effects from strain effects. To simplify the discussion, very often the average displacement due to mismatch is given, defined as the real difference from bulk metal parameters, and determined experimentally using x-ray or electron diffraction data. The average measured strain is then reported as a positive (expansion) or negative (compression) percentage deviation from bulk parameters and is usually denoted by δ or ϵ .

Strain Due to Nanoparticle Size

The variation of strain with particle size inherently comes from the surface to bulk atom ratio. The increase of the surface area to volume ratio gives rise to higher dependence on the effects of surface stress, which results in compression of the atomic arrangement to minimize the energetics of the system (surface energy).^{31,36} The dependence of strain on particle size, where smaller particles contract to a higher degree to lower the effective surface area (Figure 2a), can be modeled by the Gibbs-Thomson equation:^{12,37,38}

$$\mu(R) - \mu(\infty) = \frac{2\gamma\Omega}{R} \quad (1)$$

Where $\mu(R)$ is the molar free energy of a particle of radius, R , and $\mu(\infty)$ represents the bulk. The γ term is representative of the surface free energy of the metal atom and Ω is the bulk metal's volume per atom. Nanosystems attempt to reduce the effect of surface energy, and at smaller sizes, the surface energy term

increases. To compensate, the atom ensemble compresses.³⁹ Having a smaller size causes more compression of atoms, reducing the surface area and surface energy, where the average total displacement would tend to be more compressive versus the bulk. This is, however, complicated by capping ligands, particle shape, impurities in the metal matrix, metal identity (3d vs. 4d vs. 5d metals), support effects, and oxidation state; the latter of which is coupled to the size as well, so that this assumption may not generally hold true. In the case of pure Pt nanoparticles, for example, this is evident as strain measurements from results of both computation and experiment often do not agree, even in the type of displacement, which may not always be contraction.^{15,40-42} Sanchez et al found net expansion of the lattice parameters of nanoparticles below 10 nm of Ag, Pd, and Rh, (4d metals) whereas the heavier elements Au and Pt (5d) were compressed. Iridium was found to have similar constants to the bulk. Relativistic effects for the 5d metals and variation in d-orbital overlap were reasoned to be the source for these deviations in expected behavior.⁴⁰ Earlier work reports both expansion and compression of Pd nanoparticle lattices, presumably dependent on the presence of impurities adsorbed into or onto the Pd surfaces, such as hydrogen and oxygen.³⁶ Metal oxide and carbide compounds have also been found to have contracted parameters.⁴³ The degree of strain follows the trend of decreasing size, so while this strain effect is subtle, it's significance for catalysis is important as certain metal nanoparticle size regimes achieve better performance.^{44,45} For example, Choi et al found that sizes approaching 9 nm were optimum for oxygen reduction by PtNi octahedra.⁴⁵

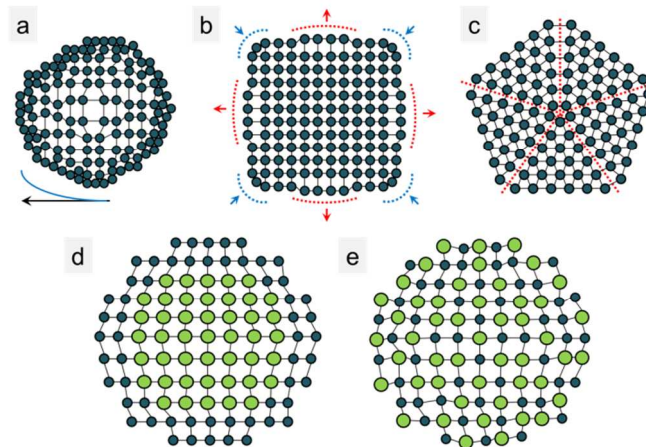


Figure 2. Illustration of the different sources of lattice strain. (a) surface relaxation due to size (compressive strain gradient), (b) anisotropic strain due to shape, (c) strain at grain boundaries due to twinning and unfilled volume, (d) strain from epitaxy in core-shell structures, and (e) strain due to alloying.

Strain Due to a 2nd Metal: Core-Shell and Alloy Structures

Starting from a relatively simple model, a single-crystalline bimetallic core-shell nanoparticle without considering the shape, size, and alloying effects (Figure 2d), the lattice mismatch between metals is given by the simple relation:

$$\frac{(core_a - shell_a)}{core_a} \times 100 \% \quad (2)$$

where a_c and a_s represent the bulk lattice constants of the core and shell metals, respectively. This is also traditionally used for describing thin films. Alternatively, lattice percent difference can be used and is given by:

$$\frac{(a_c - a_s)}{(a_c + a_s)/2} \times 100\% \quad (3)$$

The average lattice percent difference could be a more meaningful metric, providing the size of the crystal domains of the individual metal phases in a core-shell nanoparticle are on the same order of magnitude. In theory, these percentages can be thought of as the maximum amounts of strain possible at the interface, though in reality, this is unlikely to be achieved. Since both metal lattices may relax in order to accommodate the imparted strain. When the misfit between two metals is very large, epitaxial growth is forbidden in bulk film materials, it can still occur in core-shell nanoparticles; however, defects, such as edge dislocations, result in order to minimize the energy around such a highly strained interface. The strain generated by the mismatch at the interface of core-shell structures decays away from the source and could change the surface atomic displacement if the shell is thin enough. There are multiple tensor components involved in the theoretical calculation of lattice strain in a crystal. These methods have been described in several textbooks and are beyond the scope of this review.⁴⁶⁻⁴⁸ In a simplified model, the strain gradient in a line of atoms from the core to the surface of particles can be expressed as following an exponential or logarithmic function, e.g.:

$$\Delta a_n = \Delta a_{max} e^{-\frac{(m-n)a_c}{\kappa}}; \quad (0 < n \leq m) \quad (4)$$

where a_n is the atomic displacement (lattice parameter) of the n^{th} atom from the origin (center of a chain of atoms from core to surface, $n = 0$ is the origin), a_{max} is the maximum value of the relaxation (contraction for metals) at the surface (maximum lattice parameter), a_c is the bulk lattice parameter, κ is the relaxation length, and m is the total number of atoms in the linear chain in the direction of the surface (Figure 3).^{12,49} An example of the strain decay curve for core-shell structures was shown by Strasser for number of monolayers of Pt on a Cu(111) film using lattice parameters measured from electron diffraction patterns (Figure 4).¹⁰ Significant values of the average strain (between 1 and 2%) were observed for this system, even beyond a dozen deposited Pt monolayers (lattice mismatch for Pt-Cu is ~8%). At one monolayer coverage, the strain was already near half the mismatch (4-5%), but compression > 1% was observed even after ~15 monolayers of coverage, which corresponds to a thickness of around 3 nm. Wang correlated increased activity and decreasing Pt-Pt bond distance in Pd-Pt core-monolayer-shell nanoparticles of different sizes.²³ Their study is important as the mismatch between Pd and Pt is very small (<1%), yet the Pt-Pt bond distance had a linear relationship with the specific activity (decreased size increasing Pt monolayer contraction). Moreover, they effectively decoupled this from ligand effects by only changing particle size to increase strain. Montes de Oca studied the Pd shell thickness on Au cores and showed a dependence of epitaxial strain for the CO oxidation potential.¹⁶

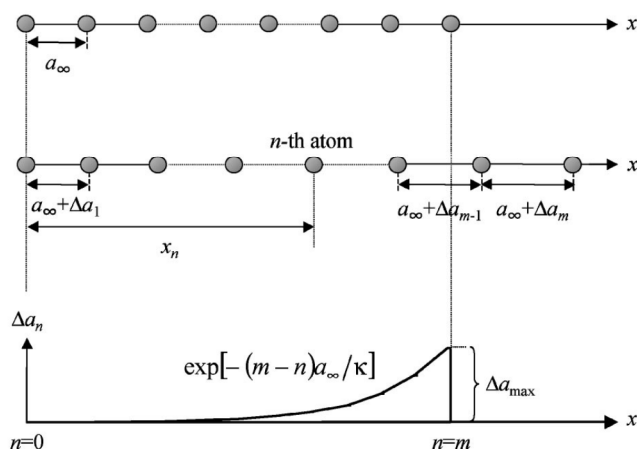


Figure 3. Schematic showing the exponential curve model for strain due to relaxation according to equation 4. Reprinted with permission from reference 49, Copyright 1999, APS.

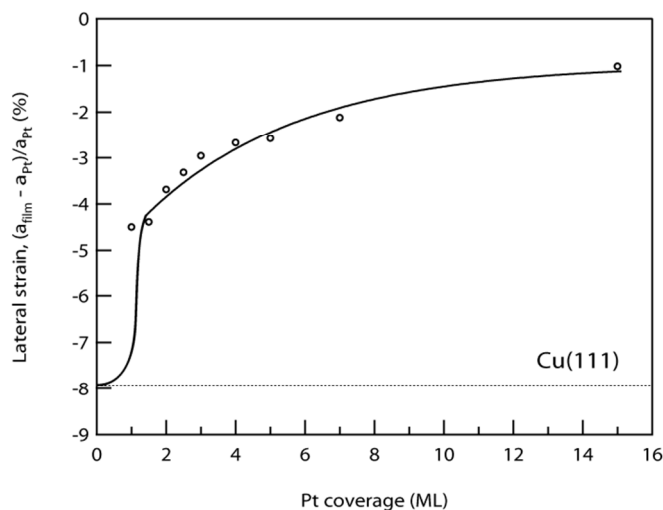


Figure 4. Plot of strain versus the number of Pt monolayers from low-energy electron diffraction (LEED) of Pt films on a Cu foil. Reprinted with permission from reference 10, Copyright 2010, NPG.

Characterization of nanocrystalline powders by X-ray diffraction reveals subtle shifts in the lattice parameters due to decreased size and increased epitaxial strain, but also, an increase in the distribution of strained parameters at smaller sizes through broadening of these peaks. The Williamson-Hall-modified Scherrer relationship gives estimates of both crystallite size and the strain distribution based on total line broadening after accounting for the instrument's effects:

$$\beta = \frac{K\lambda}{D \cos \theta} + \epsilon \tan \theta \quad (5)$$

where, D is the average size, β is the peak full width at half the maximum height, K is a shape factor, ϵ is the distribution of strain, and θ is the Bragg angle.⁵⁰⁻⁵² Due to the shifts and increased distribution of strain, as well as overlapping peaks in bimetallic structures, an accurate picture of strain of surface atoms in particular (isolated from the rest of the diffracting

phase) is challenging and has to be obtained either through help by simulation, (accounting for defects and metal diffusion), HRTEM images, X-ray absorption, or indirectly by surface-specific means such as the electronic structure shifts in X-ray photoelectron spectroscopy (XPS). Knowing the real strain and electronic structure at surfaces is especially important for catalysis applications.

The synthesis of core-shell nanoparticles can be accomplished by the mild conditions of epitaxial seed-mediated overgrowth of one metal on another, or by differences in deposition rates based on reduction potential in co-reduction methods. The resulting displacement of atoms near the interface in a core-shell structure exists over several atomic layers. In real systems, a combination of both epitaxy, and release of strain through defects will be present. The degree of the displacement, defect density, and range of the gradient in lattice parameters will depend on the lattice mismatch (identity of metals). As with surface relaxation, the decay of strain versus the distance away from the interface follows a logarithmic curve, but this is made more complex because of an added interface (metal-metal interface and metal-surface interface).

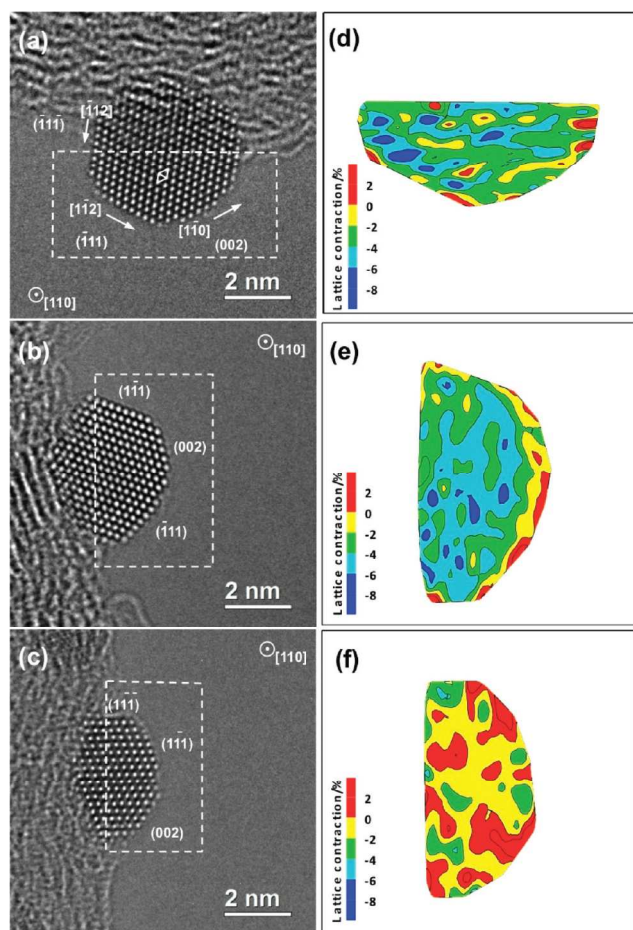


Figure 5. Alloy FePt (a,b,d,e) and Pt (c,f) nanoparticle strain maps from HRTEM analysis. Reprinted with permission from reference 15, Copyright 2012, ACS.

A variety of epitaxial overgrowth methods are available for the production of core-shell metal nanoparticles.⁵³⁻⁵⁶ Our group has primarily utilized the mild aqueous growth and overgrowth of metals using CTAB surfactant and bioorganic acid reducing

agents, such as ascorbic and citric acid, as reducing agents.^{20,22,57-59} The general method was inspired by the groups of Huang and Xu, who demonstrated the shape evolution of Au and Pd substrates by seed-mediated epigrowth.⁶⁰⁻⁶² This information was used in our synthesis and study of Au-Pd core-shell cubes and octahedra with strain-enhanced FOR activity.²⁰ Additionally, we employed shape-directing halides to create core-island-shell Pd-Rh nanoparticles with shape-control and an orderly grid-like arrangement of islands on the substrates.^{22,59} Alayoglu used a poly-ol approach in the synthesis of core-shell Ru-Pt nanoparticles.⁶³ The creation of core-shell structures containing non-precious metals via this method, however, is challenged by their low reduction potentials, high surface energy, and instability in aqueous solutions. Xia's group has addressed this issue by growing Cu epitaxially from Pd in aqueous solution using hexadecylamine, glucose, and PVP-capped Pd cubic substrates.⁵⁶ Their work is important as the lattice mismatch of the two metals is relatively high at ~7% and few defects were observed. Ni can also be grown from Pt seeds in aqueous solution by hydrazine reducing agent, owing to its better stability in base.⁶⁴ We have grown Ni epitaxially from Pd cubes and octahedra, although defects were present. The lattice mismatch for Pd-Ni is ~9%. Ping et al. produced Ag-Ni core-shell nanocubes by multi-step reaction in organic solvents at elevated temperatures.⁶⁵

Bimetallic alloy nanoparticles have been heavily studied for their improved performance in catalysis applications.^{63,66-71} Alloy nanoparticles experience lattice strain (Figure 2e), but this was seldom discussed as the major participant in catalysis mechanisms until more recent years, as it is extremely challenging to decouple it from ligand and ensemble effects. Each metal in an alloy is displaced from its normal, bulk positions, resulting in a different electronic band structure.³² Changes in the composition of alloys coincide with variations in the degree of strain for each metal atom type. The local degree of homogeneity in the mixture of metals also plays a role in this regard. Because of the complexity of alloy surfaces, many works may invoke ensemble or ligand effects (composition) for improved performance, when lattice strain could be operative as well. It is likely that the improved catalytic activity observed comes from a combination of all of the effects working synergistically. The determination of surface strain displacement of alloy nanoparticles is additionally challenged by restructuring due to metal segregation.

Alloy PtFe nanoparticles supported by carbon were synthesized by an impregnation method in a study by Gan et al.¹⁵ Strain maps were generated from HRTEM lattice images of dealloyed PtFe and pure Pt nanoparticles (Figure 5). They observed mixed expansive and compressive strain versus the bulk Pt lattice parameters, but found a core-shell strain gradient for the alloys suggesting a restructuring of the catalysts. PtCo alloy nanoparticles, also prepared by impregnation, were studied by Abruna's group.⁷² They found intermetallic ordering of the structures with an Pt-enriched shell for the particles prepared at higher annealing temperature. This led to better activity and stability for the ORR. Importantly, the activity also followed lattice contraction in addition to degree of homogeneity. Since the surface contained at least a few monolayers of Pt, ligand and ensemble effects were significantly diminished, and so it is reasonable to attribute the activity increase to compressive strain of Pt surface atoms. A similar finding was discovered previously by Strasser et al. in the dealloying of PtCu ORR catalysts.¹⁰ Their work preceded

the recent synthesis and study of record-breaking ORR catalysts based on the dealloyed Pt-skin motif, most notably, PtNi octahedra.^{44,45,73-76} Typically, shape-controlled alloy nanoparticles such as these are prepared by co-reduction of metal precursors in organic solvents. Xia's group has prepared PtNi octahedra in oleylamine and oleic acid using CO as a shape-directing agent.⁷⁵ Strasser's group prepared them via dimethylformamide (DMF), but has also used CO to control the nanoparticle size.^{73,77} Li's group produced them using a poly-ol method in benzyl alcohol/benzoic acid solution and with PVP as the capping agent.⁷⁴

Strain Due to Morphology

Morphology is an important property of metal nanocrystals that also has an intimate relationship with lattice strain due to the anisotropic nature of polyhedral geometries (Figure 2b). Shaping of nanocrystals generates structures which can strongly deviate from the ideal Wulff construction, producing high surface energy facets, vertices, and edges. The vertices and edges contain under-coordinated surface metal atoms. These dangling atoms are better stabilized by inward displacement from their usual lattice positions, resulting in an effectively higher coordination number. The surrounding atoms are likewise displaced inward to accommodate the contracted edge and corner atoms. This effect ripples outward in a strain gradient, and contributes to an opposite displacement for atoms on the faces, where the drive to lessen surface area by becoming more spherical serves to expand atoms outward (a slight outward bulging of the face atoms). From the point of view of molecular adsorption during catalysis, this is intriguing as both compressed and expanded atomic arrangements will be present on the surface, forming distinctly different areas for surface interactions. The anisotropic strain gradients on shape-controlled nanocrystals could be contributing to some of the activity enhancement observed with shape-tuned catalysts, as the effect highly depends on both the specific polyhedron geometries and size of the particles. This could indeed resolve conflicting explanations from studies in the literature.

The above shape-strain relationship has been reported in simulated x-ray diffraction patterns of three commonly encountered, low-index-faceted and face-centered-cubic nanocrystal morphologies (Figure 6).⁷⁸ Scardi et al showed how subtle features (satellite peaks) at the base of the main diffraction peaks are different between the shaped nanoparticle ensembles. For example, cubes have prominent shoulder peaks about the 200 position that were unobserved for octahedral models, showing only smooth curves. This is a unique result of the anisotropic strain gradients (corner/edge compression versus facet expansion), characteristic for each shape. According to this result, it is possible to determine the nanoparticle morphology at a global scale. This is discussed further in the characterization section.

Twinned Crystals

The more commonly encountered polycrystalline, or twinned, nanoparticle morphologies for face-centered cubic (FCC) structures are decahedra (the popular Au nanorods are essentially elongated decahedra) and icosahedra, each possessing multiple twinned boundaries. They are made up of (111)-terminated tetrahedra which meet along faces. An icosahedron has 20 faces, 30 edges, and 12 vertices from 20 tetrahedral subunits. Related in structure to the icosahedron, the twinned decahedron has 10 faces made from 5 tetrahedral

subunits, with 15 edges and 7 vertices. Since these twinned structures do not perfectly fill the volume that the atoms would normally occupy, strained structures result, with the majority of the displacement occurring along the boundaries of the tetrahedral subunits (Figure 2c).

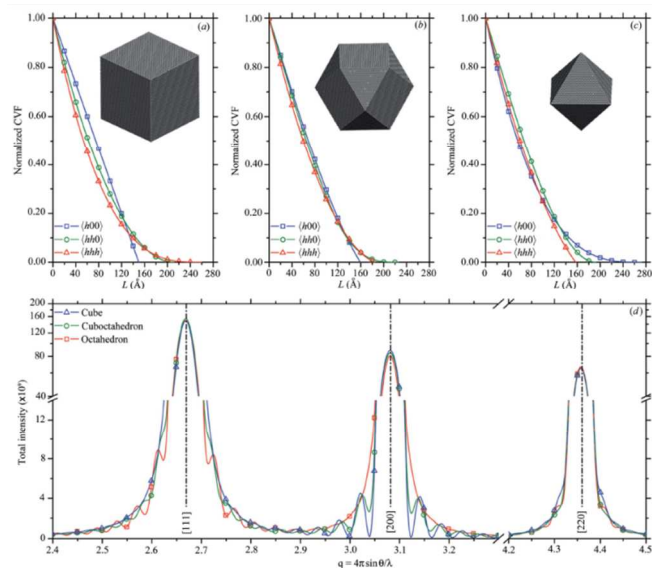


Figure 6. Modeling of x-ray diffraction patterns for differently shaped nanoparticles using the common volume function. (a) cubes, (b) cuboctahedra (c) octahedra. Simulated diffraction patterns show the unique fingerprints from satellites around the main peaks for different morphologies in (d). Reprinted with permission from reference 78, Copyright 2012, Wiley.

Their instability at small sizes makes their synthesis challenging.³ Many groups have demonstrated the synthesis⁷⁹⁻⁸⁷ and catalysis of twinned icosahedral nanoparticles.^{20,88,89} It is believed the twinned structures can result from two pathways, either from twinned seeds or from twinning of individually formed tetrahedral subunits during growth.⁸⁵ Because oxygen is believed to adsorb better on the boundaries between the crystallites, inhibition of oxidative etching by using citrate ions has been proposed in the mechanism of formation.^{81-83,85,86} Impressively, Wu et al produced alloy Pt₃Ni nanoicosahedra and attributed higher oxygen reduction activity to strain effects at edges and corners of the structures (Figure 7).⁸⁸ These particles were produced via co-reduction in oleylamine and oleic acid solution at high temperature. Some AuPt and PdPt alloy nanoparticles could also be produced using similar methods. Carbon monoxide was employed to suppress oxidative etching as a reducing agent, to restrict size as a capping agent, and to increase uniformity of the size distribution. They utilized molecular dynamics to generate models and strain maps showing both expansive and compressive atomic displacement for these particles in support of their findings. Lv et al also found higher activity for Pd icosahedra vs. other shapes in formic acid electrooxidation (FOR) and ascribed this to defects at the twinned boundaries resulting from the strain.⁸⁹ They produced these icosahedra by a polyvinylpyrrolidone (PVP) capping agent in ethylene glycol (poly-ol strategy) with ascorbic acid reducing agent. Our group has demonstrated a method to generate Pd icosahedra using cetyltrimethylammonium bromide (CTAB) surfactant and sodium citrate in aqueous solution.²⁰ We also observed

enhancement for the twinned particles over Pd octahedra and Au-Pd core-shell octahedra for this reaction, likely due to greater surface strain. Twinned decahedra have been studied less for catalysis applications, but there are computational studies discussing local highly strained regions in the structures.²¹

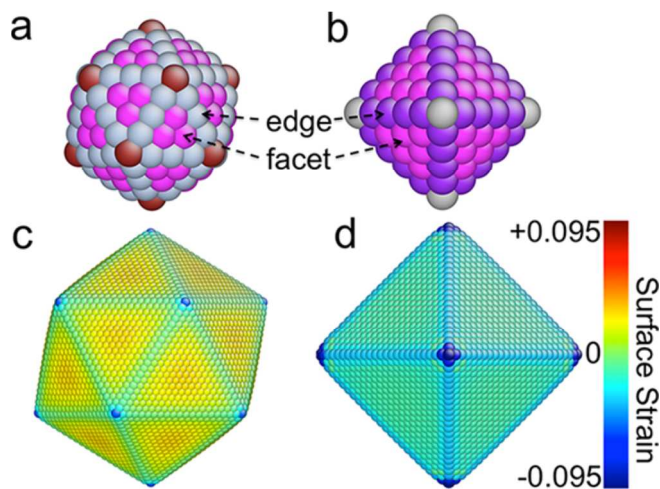


Figure 7. Crystal models and strain maps of icosahedral (a,c) and octahedral (b,d) nanocrystals. Reprinted with permission from reference 88, Copyright 2012, ACS.

Strained Archetypes of Higher Complexity

In addition to the basic strained structure types described above, a number of more sophisticated architectures have been generated in the past few years: phase-separated heterostructures, alloy-core-shell structures, core-alloy-shell structures, and core-sandwich-shell multimetallic nanostructures. Simple models for these archetypes are given in Figure 8, yet again it is noted that multiple sources of strain could be operative, for example, when controlling their shape. While the new archetypes bring with them considerable challenges in terms of their synthesis, characterization, and assignment of catalytic underpinnings, they are ideal platforms for further investigation of strain effects. Furthermore, they could be effective design concepts for the next generation of state-of-the-art electrocatalysts by offering multifaceted control of each of the important factors that modify catalytic behavior (size, shape, composition, and strain). In the synthesis of such structures, each parameter can be tuned and optimized independently from the others. This can be used to better assess their catalytic relevance and decouple them from each other.

Phase-Separated Heterostructures

Phase-separated nanoparticles consist of alternating metal phases a few nanometers in diameter in a continuous structure (Figure 8a). Our group was able to produce this archetype by prolonged solvothermal treatment of Pd-Rh core-island-shell nanoparticles (Figure 9).²² The cubic core-island-shell nanoparticles evolved into hollow cubic nanoboxes by migration of Pd from the core to fill in the island framework. To our knowledge, there are very few other examples of this type of grid-like, alternating ordering of continuous metal lattices in the literature. Each of several Pd-Rh interfaces in the structure may present strain, ligand, and ensemble effects in

catalysis. We found that while their activity for FOR fit what we expected for homogeneously alloyed structures, the mostly indirect oxidation pathway followed by the catalyst surfaces was unexpected given the nanosized Pd phases that were resolved at the surface in STEM/EDX elemental analysis. We believe this was due to compressive strain on the Pd portions from the Rh framework (Pd electronic band structure modified by the Rh). We believe this archetype could be produced for alternate metal combinations where mixed island/film growth is observed, Pt on Pd for example, and could be used to improve catalyst behavior for a particular reaction. Separate metal phases of a nanoscale surface may offer unique multi-atom catalytic ensemble sites that do not exist for homogeneous alloys, and so are exciting prospects for future studies.

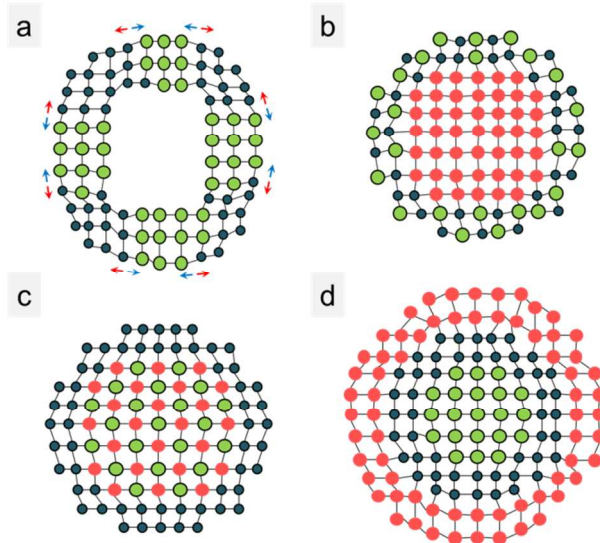


Figure 8. Illustration of more sophisticated multimetallic archetypes. (a) phase-separated heterostructure, (b) core-alloy-shell structure, (c) alloy-core-shell structure, and (d) core-sandwich-shell structure.

Trimetallic Core-Shell Nanoparticles

Core-alloy-shell nanoparticles consist of a core metal surrounded by a shell of a different metal alloy (Figure 8b). There are some works in the literature highlighting this archetype. Kang et al have synthesized dendritic core-alloy-shell Au-PdPt nanoparticles through a facile aqueous method.⁹⁰ They utilized CTAC surfactant, ascorbic acid, and hydrazine reducing agents to produce the structures, which showed appreciable activity in methanol oxidation (MOR). They compared spherical versus octahedral dendritic particles and found the latter to be more active for MOR. Sun's group has recently published a procedure for the preparation of Au-PdCu and Ag-PdCu core-alloy-shell nanoparticles using a solvothermal approach in oleylamine.⁹¹ Previous to this work, in a collaboration with Stamenkovic, among others, they exhibited Au-PtFe core-alloy-shell structures with enhanced ORR activity (Figure 10).⁹² Choi et al have impressively demonstrated shape-controlled core-alloy-shell Pd-NiPt nanoparticles using a poly-ol approach.⁹³ This was also achieved via solvothermal reaction in oleylamine.

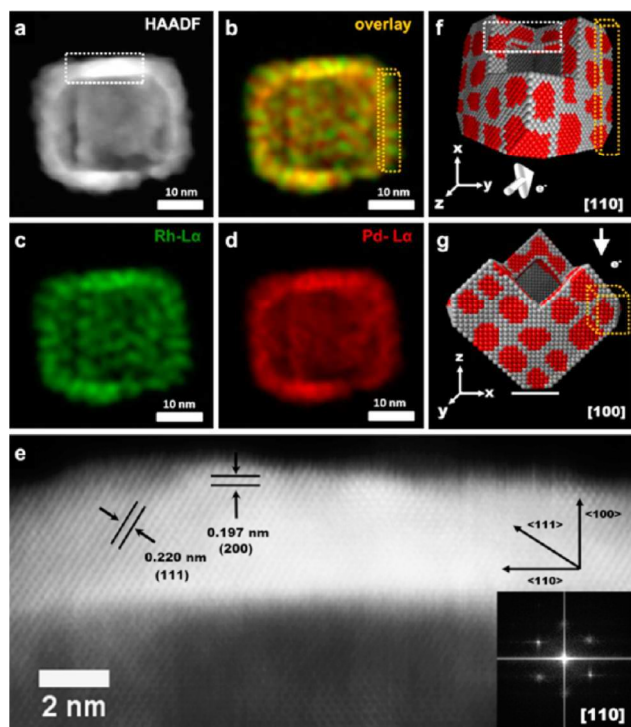


Figure 9. STEM elemental analysis of Pd-Rh phase-segregated alloy nanoboxes. (a) dark field image, (b) overlaid Pd and Rh element maps, (c) Rh map, (d) Pd map, (e) magnified shell region of image a, and (f,g) model for orientation of the nanobox. Reprinted with permission from reference 22, Copyright 2013, ACS.

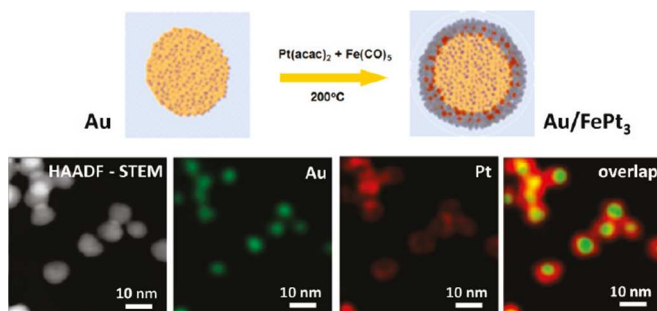


Figure 10. Synthesis scheme of Au-FePt₃ core-alloy-shell nanoparticles and corresponding elemental profiles from STEM/EDX. Reprinted with permission from reference 92, Copyright 2011, ACS.

Multimetallic alloy-core-shell structures contain a bimetallic core surrounded by a shell of another metal (Figure 8c). The afore-mentioned dealloyed, Pt-skinned catalysts could be considered simpler versions of these alloy-core-shell structures. This archetype offers the capability to tune surface strain by modification of the composition in the core, in addition to size and shell-thickness tuning. There are some examples of this structure in the literature,⁹⁴ perhaps best displayed by Ying's group. Yang et al synthesized AgPd-Pt alloy-core-shell nanoparticles using a multi-step solvothermal approach in oleylamine.¹⁸ They found these structures had improved performance over Pt/C for ORR. Previously they

reported improved ORR activity from an AuCu-Pt alloy-core-shell structure prepared similarly.¹⁷ In a computational work by Zhang et al, PdNi-Pt in an alloy-core-shell structure was predicted to have optimum oxygen binding for the ORR, where a favorable range of composition-tuning was found compared to the other Ag and Pd first-row late transition metal alloys they studied (Figure 11).⁴²

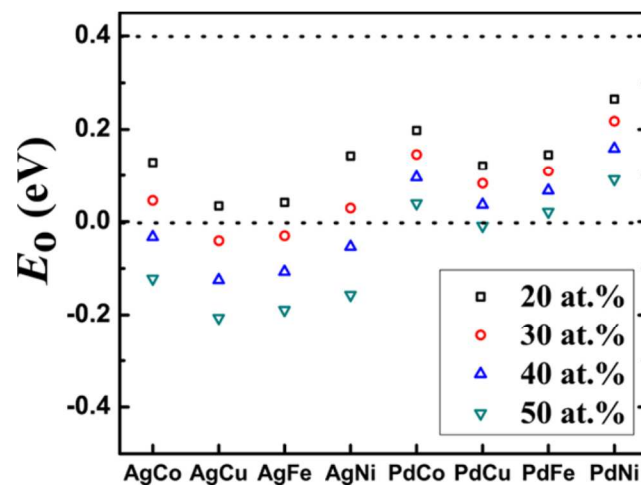


Figure 11. Results of theoretical studies of various 1st-row transition metal Ag and Pd alloys as cores in alloy-core-Pt-shell nanoparticles for oxygen reduction electrocatalysis. The target binding energy range for oxygen is shown between dotted lines, where PdNi alloy cores are predicted to be the most promising alloy-core-shell structures. Reprinted with permission from reference 42, Copyright 2013, ACS.

Core-Sandwich-Shell Nanoparticles

The last archetype discussed is the core-sandwich-shell structure (Figure 8d). Also described as “core/interlayer/shell”, “double-shelled”, or “triple-layered” nanoparticles, they consist of a metal layer sandwiched between two other metal layers in the core and shell. Some works have demonstrated the utility of this concept in the literature. Kang synthesized Ni-Au-Pt core-sandwich-shell nanoparticles by a solvothermal oleylamine route and found better durability for ORR catalysis by the Au sandwich layer.⁹⁵ Previous to this, Ferrer et al produced Au sandwiches inside core and shell Pd layers by a poly-ol method.⁹⁶ Zhang et al produced octahedral Pt-Pd-Pt double-shelled nanoparticles by forming Pt seeds from a poly-ol procedure and their subsequent coating by Pd and Pt using citric acid as reducing and capping agent in aqueous overgrowth.⁹⁷ Qiu et al devised a one-step, aqueous method for producing Ag-Co-Ni core-sandwich-shell nanoparticles reliant on ammonia borane as the reducing agent and PVP capping agent, with differences between reduction potential and magnetic permeability serving critical roles in the growth mechanism.⁹⁸ Catalytic dehydrogenation of ammonia borane had been used previously to create Au-Co-Fe core-sandwich-shell nanoparticles by Aranishi et al.⁹⁹ We have used a similar aqueous route to produce non-precious metal sandwiches of Ni between Pd and Pt layers (Figure 12).⁵⁷ We instead utilized hydrazine as the reducing agent, CTAB as the surfactant, and were able to obtain better-defined shapes by use of shape-controlled Pd substrates in a two-step, substrate growth and sandwich-shell overgrowth approach. We demonstrated the

improvement of catalyst activity for MOR by tuning the thickness of the Ni sandwich layer in our study. Additionally, the concept could be used to generate more industrially relevant smaller sizes of the core-sandwich-shell Pd-Ni-Pt nanoparticles.

Characterization of Lattice-Strained Nanoparticles

The problem of atomic resolution is a challenge facing many areas of research. As more and more applications rely on nanoscale systems and nanoscale characterization, electron microscopy has evolved to meet those new demands, with high-end electron microscopes indisputably giving the highest chemical resolution of any probe. It is possible to measure d-spacings of strained metal nanoparticles by HRTEM lattice images, and by SAED and LEED patterns. The major, and perhaps only disadvantage associated with the current stage of advanced electron microscopy techniques is low sampling. In a preeminent work by Xin, Mundy et al, a statistically more relevant analysis of ensembles of PtCo nanoparticle fuel cell electrocatalysts was accomplished by using a 5th-order aberration-corrected STEM.¹⁰⁰ The STEM electron energy loss spectroscopy (EELS) elemental profiles they produced are given in Figure 13 for a portion of ~1,000 particles they examined. Their work is possibly the best evidence of the major role lattice strain plays in the high performance of dealloyed Pt nanoparticles, as they observed at least 3 monolayers of Pt on the surface of PtCo alloy cores for the vast majority of the ensemble, negating the hypothesis for direct ligand effects, which primarily are believed to be operative for only the first 1-2 monolayers. This work was later followed by Wang's study of the ordering of annealed PtCo nanoparticle electrocatalysts, where improved activity and durability was attributed to intermetallic ordering from preparation at higher temperatures (Figure 14).⁷²

TEM is complemented by X-ray diffraction, providing global information on lattice parameters of trillions of particles in nanocrystalline powders. Higher resolution powder X-ray diffraction (HRXRD) can be done using synchrotron x-rays. Because of the current limitations toward sampling the local atomic structure of nanoparticle surfaces, specifically at global scales, development of the theory and modeling of diffraction in combination with experimental HRXRD and molecular dynamics (MD) simulations is believed to bring about significant progress in accurately assessing and quantifying surface lattice strain.¹⁰¹ In collaboration with Scardi's group we have made recent strides in this regard for single component systems of shaped Pd nanocrystals.¹⁰² The strain due to the cubic morphology was observed for Pd nanocubes using the Advanced Photon Source at Argonne National Laboratory. The fringes of the 200 peak provided experimental validation for their predictions (previously discussed in this review), of an anisotropic strain gradient due to the shape, and MD simulations resulted in detailed strain maps for the structures (Figure 15). The unique diffraction patterns of shaped semiconductor crystals have also been studied by Gordon et al recently.¹⁰³

It worth mentioning that according to these results, the different morphologies could be determined by the XRD patterns. HRXRD could be further used to 'image' the averaged nanocrystal shape and atomic structure on a global scale. The current limitation for implementation of this technique is that current synthesis methodologies do not meet the requirement of high uniformity in shape (>98%) and tight size distributions (\pm few nm) to observe this effect. However, as progress in

synthesis steadily improves, powder XRD may prove to be ideal in quantitatively assessing the global shape yield, by fitting these simulated patterns to real diffraction data. Combining powder XRD with simulations could further be used to more accurately 'image' and generate atomic-level strain maps for the global nanoparticle ensemble. We note here that coherent X-ray diffraction (CXD) of single crystals has also been used to map surface strains, however, like TEM, this technique is limited by low sampling, and has the added requirement of larger grain sizes (>60 nm).¹⁰⁴

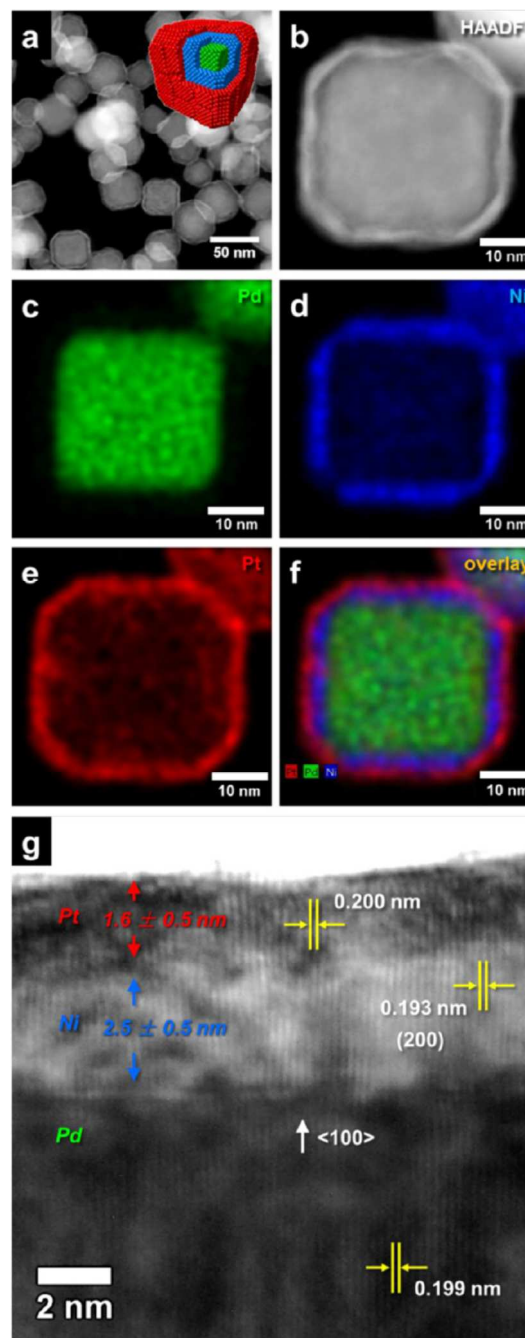


Figure 12. (a-f) HAADF/STEM/EDX images of core-sandwich-shell Pd-Ni-Pt nanoparticles and HRTEM image in (g). Reprinted with permission from reference 57, Copyright 2014, ACS.

Synthesis Challenges and Concerns for Catalysis

The development of the synthesis of metal nanoparticles will ultimately drive their use in applications, however, there are concerns that should be addressed in future work to better facilitate progress for catalysis applications. Current challenges facing this field lie in both synthesis and evolution of structure under catalysis conditions and in the isolation of the strain effect from the other essential parameters that dictate catalytic activity. There are also some limitations of the strain effect due primarily to defect generation and metal diffusion. This further complicates the prediction of stable and active strained nanoparticle architectures. Each of these challenges is described below.

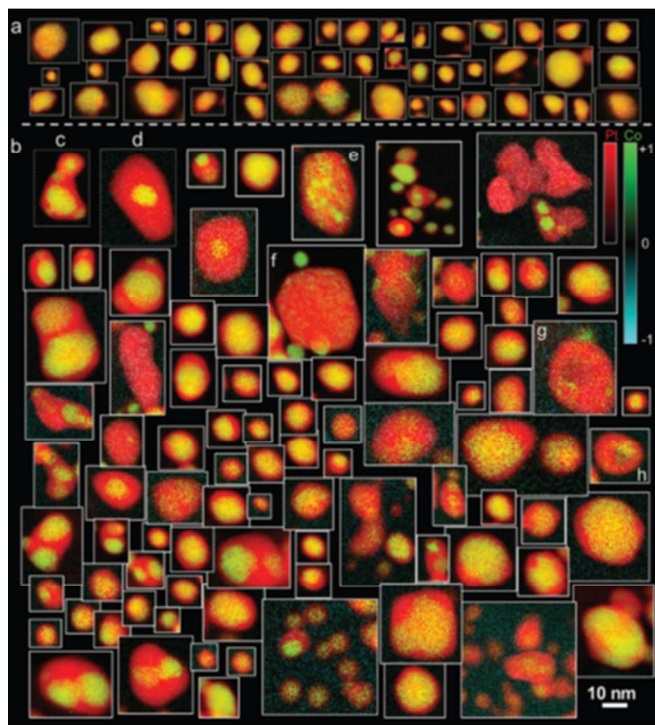


Figure 13. STEM electron energy loss spectroscopy (EELS) analysis of PtCo nanoparticles before and after electrocatalysis conditions. Reprinted with permission from reference 100, Copyright 2012, ACS.

Better Control of Structure

The rational synthesis of lattice-strained nanoparticles with atomic-level control of strain will only be possible if the size, shape, and composition can be easily tuned independent of one another. Future research should be focused on the control of both shape and composition at smaller sizes. This is a great challenge for smaller particles as there is often no possibility to impart shape in a 2nd growth step and so control must be established earlier, during the nucleation stage, if it is to occur at all. This is quite difficult for smaller sized particles, which prefer the thermodynamic Wulff polyhedra (truncated octahedra) of mixed faceting to minimize surface energy. There are several excellent reviews that discuss the use of molecular adsorbates for the purpose of shape-control that can be consulted, perhaps best summarized by Sau¹⁰⁵ and Chen.¹⁰⁶ The use of halides, in particular, is popular in the production of

cubic (100)-terminated nanocrystals.¹⁰⁷ Octahedra terminated by (111) surfaces are often obtained by the use of citrate¹⁰⁸ in aqueous solution or by organic capping agents, such as DMF. Sulfur anions have been used to cap Au surfaces to control shape as well.¹⁰⁹ Gases such as O₂ were bubbled into growth solutions to control shape by oxidative etching of 100 surfaces assisted by Cl⁻ ions to promote (111) faceting.^{110,111} The use of carbon monoxide gas for size confinement and shape control of nanoparticles has been demonstrated by many groups, by either bubbling, or introduction of transition metal-carbonyls as a CO source,^{20,73,77,112-115} however, this may be difficult for aqueous strategies, where metal carbonyls are generally only slightly soluble. Metal ad-atoms, such as Ag, are often used in the seed-mediated growth of shaped Au and Pd nanoparticle synthesis, and quite recently Ni has served a role in the production of Pt multicube structures.¹¹³ Despite these advances, the methodologies available for control of shape are still somewhat limited, and so this should be addressed in future research.

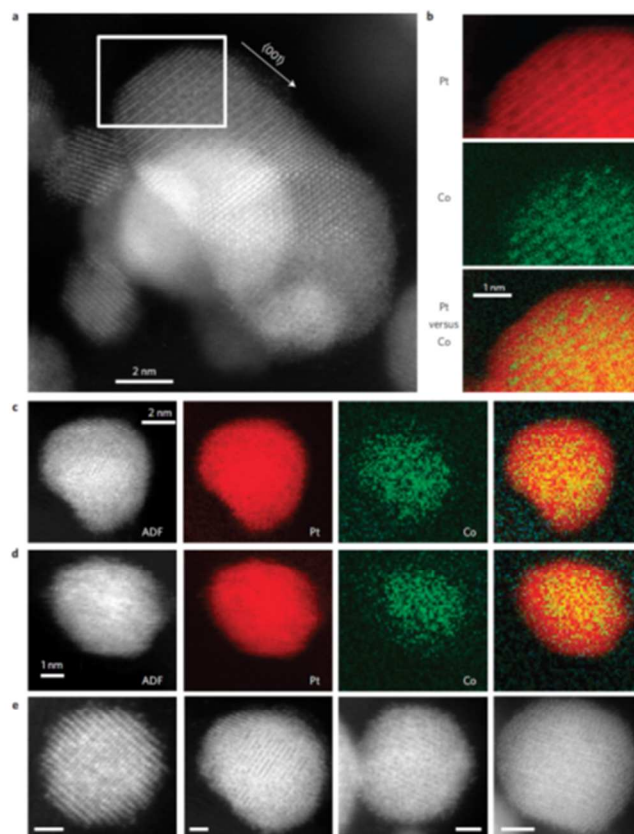


Figure 14. Atomic resolution STEM/EELS analysis of PtCo intermetallic nanoparticles. Reprinted with permission from reference 72, Copyright 2013, NPG.

A similar challenge is present for shape control of alloy nanoparticles. Co-reduction of metal precursors to create homogeneous alloys is challenging, as the reduction potentials must be matched, otherwise core-shell structures result. Slight changes to synthesis conditions by shaping additives may alter these potentials by forming complexes with metal precursors, removing the control for composition. It is also rare that more than one shape of alloy nanocrystals can be generated by simple adjustment of the same general synthesis route.¹¹⁴ This may require a different approach. Higher-index faceted nanoparticles

are also rarely encountered in the literature, despite their multiple stepped surfaces offering a way to increase activity.¹¹⁶⁻¹²⁴ Recent advances have been made in this general direction, for example, in the production of rhombic dodecahedral (110)-terminated alloy nanocrystals;^{125,126} however, the detailed mechanisms of formation of these morphologies are still a subject for future research. Impressively, a recent study has shown the shape control of a trimetallic alloy of PtNiCu nanoparticles made by an impregnation method, also with efficient oxygen reduction behavior.¹²⁷ More effort should be directed to this purpose for solution-based approaches.

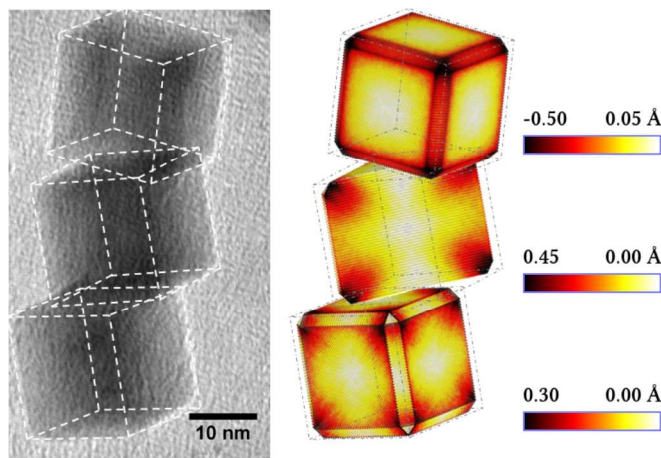


Figure 15. Displacement maps showing the anisotropic strain gradients of cubic nanocrystals relative to all surfaces (top), for the (110) cross-section (middle), and on each facet (lower). (a) Reprinted with permission from reference 102, Copyright 2015, APS.

Atomic Level Control of Layer Thickness

To accurately measure the lattice strain at the surface of metal nanocrystals, precise control over the number of monolayers of metals must be acquired. Strain could significantly affect the heteroepitaxial growth mode, especially for the first few layers, and this may prove difficult for synthesis of highly strained core-shell nanoparticles.¹²⁸ The Xia group has met this challenge for low mismatching metals by the recent development of synthesis methodology of atomic layer deposition on metal nanocrystal substrates (Figure 16).¹²⁹⁻¹³¹ They were able to control the number of monolayers of Pt on Pd cubes and octahedra, and used this to optimize catalytic activity for ORR.^{129,131} The control of layer thickness while simultaneously controlling shape is another related challenge. For example, if the substrate of core-shell nanoparticles is a small seed taking a Wulff-shape, the creation of cubes and octahedra during overgrowth will result in a gradient in the number of monolayers across the surface of facets because of the anisotropy of the two different shapes (mismatch of seed shape). This should likewise produce a strain gradient across the facets, competing with the strain inherent in the shape. Decoupling the effects of shape and strain on catalysis would be difficult in this case, as we noted in our study of formic acid oxidation activity of Au-Pd core-shell nanocubes and nanooctahedra.²⁰ Park et al. recently examined an analogous system of Pt overgrowth on truncated Pd octahedra.¹³¹ They were able to control the overgrowth to recapitulate a truncated core-shell form, and also produced sharper, fully-filled

octahedral core-shell structures by dropwise versus one-step injection of precursors in poly-ol versus aqueous methods, respectively. They then compared ORR activity for the two systems and found better activity for the sharper octahedra of the aqueous method, and attributed this to the increased (111) surfaces, though strain of the high-energy vertices could not be decoupled from the facet argument.

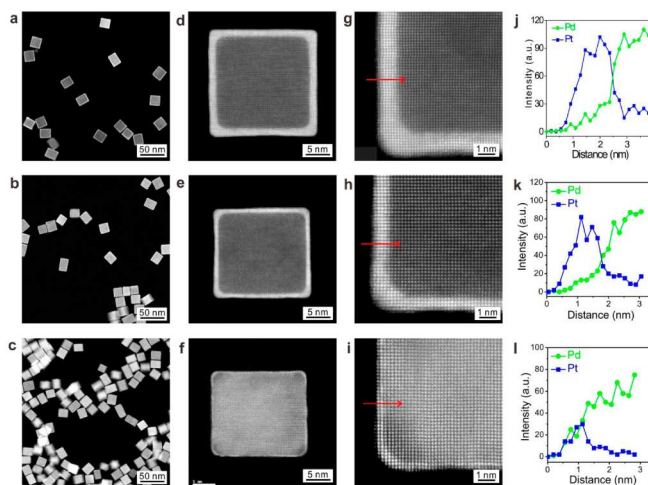


Figure 16. Control of monolayer thickness of Pd-Pt nanocubes. TEM images of 6, 4, and 1 monolayers of Pt on Pd cubes (top to bottom). Reprinted with permission from reference 129, Copyright 2014, ACS.

Catalyst Preparation and Capping-Agent-Free Synthesis

The synthesis of nanoparticles without capping agents would greatly benefit catalysis applications.^{132,133} There are some groups promoting nanoparticle synthesis using organic solvents as capping-agent-free methods where the particles are stabilized by the solvent molecules.⁷³ Since they are not stabilized by the conventional capping agents, the particles are instead captured on a support immediately after their synthesis. While a traditional capping agent is not employed, it remains clear that there is a capping effect of the organic solvent to produce the resulting morphology, and the same cleaning may be necessary because of this and differing solvents in catalysis applications. Future work should be directed at better control of the size, shape, and composition of metal nanoparticles without the use of capping agents, but this attractive end goal is somewhat paradoxical, as these capping agents play perhaps the most important role in much of the atomic-level control of structures discussed throughout this review. Great strides have been made in the removal of capping agents, in addition to the development of greener chemical synthesis without them, and so this is a possible alternative. We showed how sacrificial coating and subsequent etching of Cu₂O could be used to rid the surface of catalytic nanoparticles of shaping agents such as iodide.⁵⁹ A typical neutral polymer capping agent utilized in poly-ol methods, polyvinylpyrrolidone (PVP) has been shown to be removed by conversion into a more labile cationic polymer via Meerwein salts.¹³⁴ Chen et al used ionic liquids with high O₂-solubility to enrich the local O₂ concentration in order to improve the ORR activity of nanoframe catalysts.^{126,135,136} Nanoparticle catalysis could be strongly influenced by capping agents and preparation methods, and so future research should also be directed at diversifying these

capping agent removal strategies, as well as the synthesis without them. Our group has successfully been able to create shape-controlled multimetallic nanoparticles in aqueous solution. Ionic capping agents in aqueous solution may prove better for shape-control because of better surfactant self-assembly and could offer ease of capping agent removal by a weaker electrostatic interaction. However, the future challenge for aqueous systems lies in achieving this high level of control at smaller sizes.

Post-Synthetic Evolution of Structure

The post-synthetic restructuring of metal nanoparticles from diffusion of metals is perhaps the greatest challenge to lattice-strain control of activity. This phenomenon is prevalent at nanoscales and many of the high performance ORR catalysts are derived through some dealloying or restructuring of the surface. This means that the most active structures are not synthesized directly, but arise due to the chemical environment of different catalysis conditions. While strained structures can certainly be synthesized, there is no guarantee it will be stable in the harsh conditions of electrocatalysis, though the dealloyed M-Pt structures have high durability. The rational design of metal nanoparticle electrocatalysts that are active and stable in reaction conditions is a worthy topic for research. Future research should be aimed at the direct synthesis of strained architectures, as well as, at taking further advantage of catalytic restructuring to produce more active architectures.

Metal nanoparticle restructuring occurs due to the conditions they can be exposed to in fuel cell electrocatalysis electrolyte solutions. Pourbaix diagrams show the stability (nobility) of late transition metals under different potentials and pH in aqueous solutions.¹³⁷ Metals are shown here to be stable, completely or partially dissolved, or passivated by hydrides or hydroxides depending on their nobility. These plots are useful in predicting stability of metal nanoparticles in catalysis conditions. An important parameter that governs composition changes and restructuring in metal nanoparticles is metal segregation energy.¹³⁸⁻¹⁴² Large tables can be formulated that allow for predictive maps of stable core-shell configurations (Figure 17).^{141,142} The segregation energy is correlated to fundamental properties such as atomic size, cohesive energy, vapor pressure, and surface energy.¹⁴¹⁻¹⁴⁴ Atomic size and cohesive energy were found to be most useful in predicting preferences, where smaller atoms with more cohesive energy nearly always having a preference for the core.¹⁴² Though these preferences in core-shell structures are good for a first guess, these properties can change due to chemical environments. This was studied for bimetallic systems of Pd, Rh, and Pt by Tao et al.^{145,146} They saw metal diffusion leading to restructuring of nanoparticles (different core-shell preferences) due to either oxidative or reducing gas environments. They found that this most likely was driven by heats of formation of oxides and the surface energy of the different metals. It would be useful for future research to generate maps of stable core-shell configurations under specific conditions the catalytic application, for example, in fuel cell electrocatalysis.

There is a relationship between nanoparticle size and the amount of leaching that occurs, where generally smaller sizes are more stable and tend not to leach as much non-precious metal to form porous structures.¹⁴⁷ Less porous nanoparticles of PtNi were observed when the size was restricted to below 10 nm in a study by Gan et al. This was also dependent on the surrounding atmosphere of gas, and porosity was delayed by reducing exposure of the nanoparticles to oxygen. In another

study by Gan, anisotropic growth leading to the formation of Ni-enriched (111)-facets resulted in structure changes due to leaching of Ni from these facets of octahedral PtNi particles (Figure 18).¹⁴⁸ High-performing rhombic dodecahedral PtNi nanoframe ORR catalysts were formed via this facet-specific etching similarly.¹²⁶ Rhombic dodecahedral PtCu nanosheets synthesized by Jia et al as formic acid oxidation catalysts were also found to have an excavated structure, however, these structures were believe to be formed directly through an as yet unknown mechanism (Figure 19).¹²⁵ Their method could offer an advantage in control of the non-precious metal alloy composition incorporated in the directly synthesized hollow structure, prior to any restructuring in the conditions of electrocatalysis.

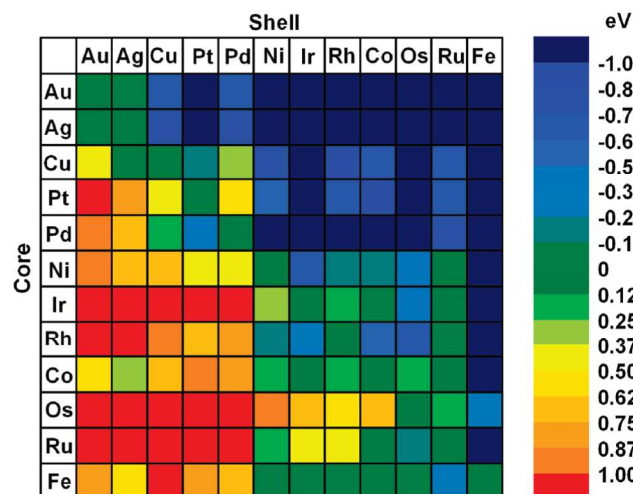


Figure 17. Calculated segregation energies and core-shell preferences for late transition metal nanoparticles arranged by d-electron filling. Reprinted with permission from reference 142, Copyright 2009, ACS.

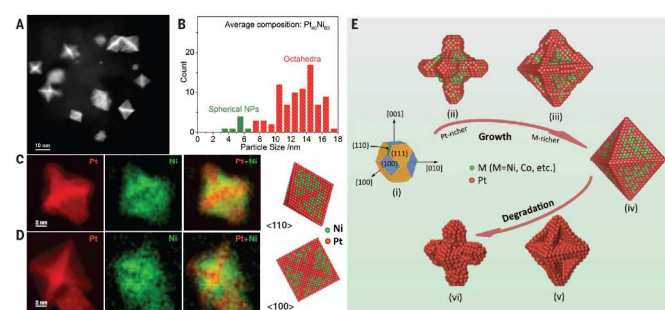


Figure 18. Scheme and STEM/EDX imaging of anisotropic growth of PtNi nanooctahedra and restructuring in reaction conditions. Reprinted with permission from reference 148, Copyright 2014, AAAS.

Recently our group has studied migration of Au into Pd shells in shaped core-shell nanocrystals during electrocatalysis.¹⁴⁹ Gold has a preference for the shell in core-shell structures with Pd, primarily due to lower surface energy. Furthermore, Au diffusion into the shell benefits the structure by relaxing the strain at the interface from the lattice misfit. Under the potential cycling conditions of formic acid electrooxidation, mixing of Au into the Pd shell led to

decreased performance, by increasing the amount of Au surface sites. The restructuring of the particles was found to be dependent on the shell thickness, where thicker shells were less affected by the increased composition of Au at surfaces due to slower diffusion times. Likewise, we also found that acidic electrocatalysis conditions causes the migration and removal of non-precious metals in core-shell structures, however, these structures could be stabilized for catalysis in alkaline electrolyte.⁵⁷ Future work at understanding multimetallic nanoparticle restructuring in catalytic conditions is currently underway, as it challenges the concept strain-tuned catalysis.

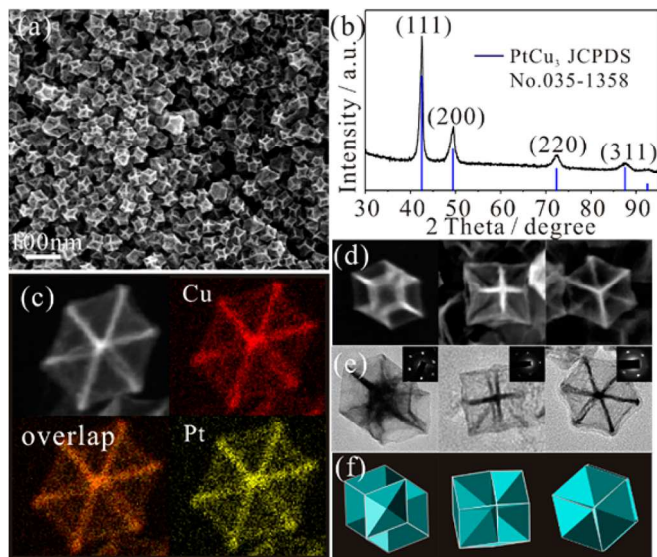


Figure 19. STEM elemental analysis and X-ray diffraction of excavated PtCu rhombic dodecahedral nanosheet electrocatalysts. Reprinted with permission from reference 125, Copyright 2014, ACS.

Limitations of the Lattice Strain Effect

For some late transition metals as matrix elements, the d-band model is quite reliable for predicting catalytic activity, however, the validity of the model is still a topic for research.^{27,28} This is likely because of the inherent complexity of reactions on metal surfaces, where many different binding species may compete for the main role in the rate of reaction.²⁸ Not surprisingly, there are exceptions even for Pt. It has been observed in specific cases that both expansion and compression of surface atoms of Pt via lattice strain from sub-surface metals can lead to similar shifts in the d-band center, resulting in improved catalytic activity for both situations.²⁵ This was the case for Ag and Cu subsurface layers, where Cu compressed the Pt surface, and conversely, Ag expanded the Pt surface. It was reasoned that this discrepancy could be due to the differences in d-orbital overlap from the 3d and 4d metals to the 5d metal. This discrepancy suggests that the binding energy of adsorbate intermediates may be a better metric in predicting catalytic activity. Volcano plots following the classical Sabatier principle have been made relating binding energy (activity) to various parameters such as composition and d-band center.¹⁵⁰ It would also be useful to map out such volcano type relations for shape, strain, and composition. It may be possible, for example to obtain multiple types of the same high-performing metal nanoparticle catalysts by tuning size, monolayer thickness, or shape in addition to composition tuning of cores in core-shell

structures. To our knowledge, there is no work which simultaneously and independently connects and assigns the effect of each of these parameters to the catalytic activity, likely because synthesis methodologies are not yet versatile enough to generate a complete set of particle controls for this purpose.

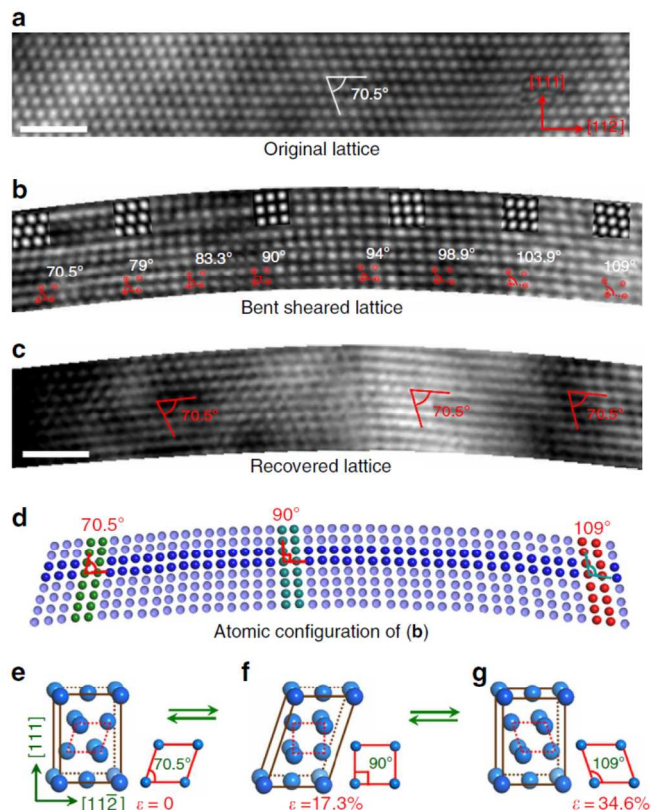


Figure 20. Unit cell flip in bent Ni nanowires. Reprinted with permission from reference 152, Copyright 2013, NPG.

The release of strain through defects will lessen the strain effect on catalysis by relaxing the structure. Several mechanisms of strain release in nanoscale systems have been studied.¹⁵¹⁻¹⁵³ One such case was examined by Wang et al, where a nearly $\sim 40^\circ$ reversible flip in the unit cell of Ni was observed when Ni nanowires were bent (Figure 20).¹⁵² Size-dependent phase transitions, only possible at nanoscales, have also been shown for Au.¹⁵⁴ If excessive strain exists in nanoparticles it could be relaxed by these mechanisms and thus is a problem to be overcome for catalysis applications. In work by Bhattarai, defect generation at the interface of Au-Pd nanoparticles was studied by electron microscopy.^{19,116} They found that Shockley partial dislocations, stacking faults, and misfit dislocations resulted in a more relaxed structure (lattice mismatch of $\sim 5\%$ for the Au-Pd system) after the synthesis. They also showed that Au diffused into the growing Pd shell to further accommodate the strained Pd overlayers. A similar finding was revealed by Kwon et al for heterogeneous overgrowth of Au on PtCo alloy seeds in the synthesis of dumbbell structures, where they found many slipping plane defects in the Au layers near the interface.¹⁵³ Gutkin et al have studied misfit dislocations in various nanostructures, suggesting that the presence of voids may stabilize strain in theory, by lessening these dislocations in hollow core-shell nanoparticles.^{155,156} Unit cell rearrangements, defect generation,

and diffusion of metals around the interface suggested by these studies are significant limitations for implementing strain control for catalysis. Additionally, the decay of strain away from the interface itself may prove to be less significant for metal combinations with low lattice mismatch and large numbers of monolayers. High-mismatching systems may prefer to relax through one or many of these mechanisms reducing strain similarly for thicker coatings in core-shell systems. This all may diminish the importance of the strain effect, and so more work can be directed to understanding and addressing each of these issues to assess what the real limits are for the many multimetallic late transition metal core-shell catalyst systems that can be proposed.

Conclusions and Outlook

We have defined and described the different sources of lattice strain in metal nanoparticle systems. We discussed the recent study in electrocatalysis by these structures and highlighted the synthesis routes and achievements in recently generated strained architectures. We have shown some novel archetypes that have emerged from this field, and how they may capitalize on the simpler designs. The more sophisticated architectures offer platforms to study lattice strain, as well as provide handles for tuning the important catalysis parameters independently from each other. The recent advance of electron microscopy and diffraction techniques were highlighted in the characterization of strained nanostructures. The synthesis challenges and concerns for catalysis relevant to strained architectures were then discussed. The major limitations of the strain effect, in metal diffusion and defect generation were discussed. Future efforts should be directed toward filling the library of nanoparticle structures with more sophisticated strained structures and assessing the stability of such structures in catalysis conditions. The real limits of the strain effect should also be elucidated. We believe the field holds great promise if all of these challenges are met, and we expect a new generation of nanoparticle catalysts will arrive with those discoveries. The building up of strain in metal nanoparticles could prove as an especially efficient design concept for zero-emission, sustainable energy storage and conversion technologies, and we look forward to contributing more to this exciting area of research in the coming years.

Acknowledgements

We would like to thank Boston College for funding this research.

Notes and References

^a Boston College Chemistry Department, Merkert Chemistry Center, 2609 Beacon St, Chestnut Hill, MA, 02467, USA

- (1) Haxha, V.; Migliorato, M. A. *Journal of Physics: Conference Series* **2010**, *242*, 012001.
- (2) Wu, J.; Li, P.; Pan, Y.-T.; Warren, S.; Yin, X.; Yang, H. *Chemical Society Reviews* **2012**, *41*, 8066.

- (3) Baletto, F.; Ferrando, R. *Reviews of Modern Physics* **2005**, *77*, 371.
- (4) Mavrikakis, M.; Hammer, B.; Nørskov, J. K. *Phys. Rev. Lett.* **1998**, *81*, 2819.
- (5) Kitchin, J. R.; Nørskov, J. K.; Barteau, M. A.; Chen, J. G. *Physical Review Letters* **2004**, *93*, 156801.
- (6) Richter, B.; Kuhlbeck, H.; Freund, H. J.; Bagus, P. S. *Physical Review Letters* **2004**, *93*, 026805.
- (7) Kibler, L. A.; El-Aziz, A. M.; Hoyer, R.; Kolb, D. M. *Angewandte Chemie International Edition* **2005**, *44*, 2080.
- (8) Cha, W.; Song, S.; Jeong, N. C.; Harder, R.; Yoon, K. B.; Robinson, I. K.; Kim, H. *New Journal of Physics* **2010**, *12*, 035022.
- (9) Schnur, S.; Groß, A. *Physical Review B* **2010**, *81*, 033402.
- (10) Strasser, P.; Koh, S.; Annyev, T.; Greeley, J.; More, K.; Yu, C.; Liu, Z.; Kaya, S.; Nordlund, D.; Ogasawara, H.; Toney, M. F.; Nilsson, A. *Nat Chem* **2010**, *2*, 454.
- (11) Bagus, P. S.; Wieckowski, A.; Freund, H. *Computational and Theoretical Chemistry* **2012**, *987*, 22.
- (12) Beyerlein, K. R.; Snyder, R. L.; Li, M.; Scardi, P. *Journal of Nanoscience and Nanotechnology* **2012**, *12*, 8554.
- (13) Fairclough, S. M.; Tyrrell, E. J.; Graham, D. M.; Lunt, P. J. B.; Hardman, S. J. O.; Pietzsch, A.; Hennies, F.; Moghal, J.; Flavell, W. R.; Watt, A. A. R.; Smith, J. M. *The Journal of Physical Chemistry C* **2012**, *116*, 26898.
- (14) Feng, Y.; He, J.; Wang, H.; Tay, Y. Y.; Sun, H.; Zhu, L.; Chen, H. *J. Am. Chem. Soc.* **2012**, *134*, 2004.
- (15) Gan, L.; Yu, R.; Luo, J.; Cheng, Z.; Zhu, J. *The Journal of Physical Chemistry Letters* **2012**, *3*, 934.
- (16) Montes de Oca, M. G.; Plana, D.; Celorrio, V.; Lazaro, M. J.; Fermín, D. J. *The Journal of Physical Chemistry C* **2012**, *116*, 692.
- (17) Yang, J.; Chen, X.; Yang, X.; Ying, J. Y. *Energy & Environmental Science* **2012**, *5*, 8976.
- (18) Yang, J.; Yang, J.; Ying, J. Y. *ACS Nano* **2012**, *6*, 9373.
- (19) Bhattarai, N.; Casillas, G.; Ponce, A.; Jose-Yacamán, M. *Surf. Sci.* **2013**, *609*, 161.
- (20) Kuo, C.-H.; Lamontagne, L. K.; Brodsky, C. N.; Chou, L.-Y.; Zhuang, J.; Sneed, B. T.; Sheehan, M. K.; Tsung, C.-K. *ChemSusChem* **2013**, *6*, 1993.
- (21) Patala, S.; Marks, L. D.; Olvera de la Cruz, M. *The Journal of Physical Chemistry C* **2013**, *117*, 1485.
- (22) Sneed, B. T.; Brodsky, C. N.; Kuo, C.-H.; Lamontagne, L. K.; Jiang, Y.; Wang, Y.; Tao, F.; Huang, W.; Tsung, C.-K. *J. Am. Chem. Soc.* **2013**, *135*, 14691.
- (23) Wang, X.; Orikasa, Y.; Takesue, Y.; Inoue, H.; Nakamura, M.; Minato, T.; Hoshi, N.; Uchimoto, Y. *J. Am. Chem. Soc.* **2013**, *135*, 5938.
- (24) Oezaslan, M.; Hasché, F.; Strasser, P. *The Journal of Physical Chemistry Letters* **2013**, *4*, 3273.
- (25) Kaya, S.; Friebe, D.; Ogasawara, H.; Annyev, T.; Nilsson, A. *Journal of Electron Spectroscopy and related Phenomena* **2013**, *190*, Part A, 113.
- (26) Hwang, S. J.; Kim, S.-K.; Lee, J.-G.; Lee, S.-C.; Jang, J. H.; Kim, P.; Lim, T.-H.; Sung, Y.-E.; Yoo, S. J. *J. Am. Chem. Soc.* **2012**, *134*, 19508.
- (27) Xin, H.; Linic, S. *The Journal of Chemical Physics* **2010**, *132*, 221101.
- (28) Yu, T. H.; Hofmann, T.; Sha, Y.; Merinov, B. V.; Myers, D. J.; Heske, C.; Goddard, W. A. *The Journal of Physical Chemistry C* **2013**, *117*, 26598.
- (29) Nørskov, J. K.; Bligaard, T.; Rossmeisl, J.; Christensen, C. H. *Nat Chem* **2009**, *1*, 37.
- (30) Kitchin, J. R.; Nørskov, J. K.; Barteau, M. A.; Chen, J. G. *The Journal of Chemical Physics* **2004**, *120*, 10240.
- (31) Shiihara, Y.; Kohyama, M.; Ishibashi, S. *Physical Review B* **2013**, *87*, 125430.
- (32) Hammer, B.; Nørskov, J. K. In *Advances in Catalysis*; Bruce C. Gates, H. K., Ed.; Academic Press: 2000; Vol. Volume 45, p 71.
- (33) Knözinger, H.; Kochloefl, K. In *Ullmann's Encyclopedia of Industrial Chemistry*; Wiley-VCH Verlag GmbH & Co. KGaA: 2000.

- (34) Greeley, J.; Stephens, I. E. L.; Bondarenko, A. S.; Johansson, T. P.; Hansen, H. A.; Jaramillo, T. F.; Rossmeisl, J.; Chorkendorff, J.; Nørskov, J. K. *Nat Chem* **2009**, *1*, 552.
- (35) Friebel, D.; Viswanathan, V.; Miller, D. J.; Anniev, T.; Ogasawara, H.; Larsen, A. H.; O'Grady, C. P.; Nørskov, J. K.; Nilsson, A. *Journal of the American Chemical Society* **2012**, *134*, 9664.
- (36) Qi, W. H.; Wang, M. P. *Journal of Nanoparticle Research* **2005**, *7*, 51.
- (37) Wasserman, H. J.; Vermaak, J. S. *Surf. Sci.* **1972**, *32*, 168.
- (38) Campbell, C. T.; Parker, S. C.; Starr, D. E. *Science* **2002**, *298*, 811.
- (39) Woltersdorf, J.; Nepijko, A. S.; Pippel, E. *Surface Science* **1981**, *106*, 64.
- (40) Sanchez, S. I.; Small, M. W.; Bozin, E. S.; Wen, J.-G.; Zuo, J.-M.; Nuzzo, R. G. *ACS Nano* **2012**, *7*, 1542.
- (41) Solliard, C.; Flueli, M. *Surf. Sci.* **1985**, *156*, Part 1, 487.
- (42) Zhang, X.; Lu, G. *The Journal of Physical Chemistry Letters* **2013**, *5*, 292.
- (43) Fukuhara, M. *Physics Letters A* **2003**, *313*, 427.
- (44) Zhang, C.; Hwang, S. Y.; Peng, Z. *Journal of Materials Chemistry A* **2014**, *2*, 19778.
- (45) Choi, S.-I.; Xie, S.; Shao, M.; Lu, N.; Guerrero, S.; Odell, J. H.; Park, J.; Wang, J.; Kim, M. J.; Xia, Y. *ChemSusChem* **2014**, *7*, 1476.
- (46) Ramesh, K. T. *Nanomaterials: Mechanics and Mechanisms*; Springer, 2009.
- (47) Nye, J. F. *Physical Properties of Crystals: Their Representation by Tensors and Matrices*; Oxford University Press, 1985.
- (48) Newnham, R. E. *Properties of Materials: Anisotropy, Symmetry, Structure*; Oxford University Press, 2004.
- (49) Ishikawa, K.; Uemori, T. *Physical Review B* **1999**, *60*, 11841.
- (50) Patterson, A. L. *Physical Review* **1939**, *56*, 978.
- (51) Stokes, A. R.; Wilson, A. J. C. *Proceedings of the Physical Society* **1944**, *56*, 174.
- (52) Williamson, G. K.; Hall, W. H. *Acta Metallurgica* **1953**, *1*, 22.
- (53) Fan, F.-R.; Liu, D.-Y.; Wu, Y.-F.; Duan, S.; Xie, Z.-X.; Jiang, Z.-Y.; Tian, Z.-Q. *J. Am. Chem. Soc.* **2008**, *130*, 6949.
- (54) Habas, S. E.; Lee, H.; Radmilovic, V.; Somorjai, G. A.; Yang, P. *Nature Materials* **2007**, *6*, 692.
- (55) Jiang, M.; Lim, B.; Tao, J.; Camargo, P. H. C.; Ma, C.; Zhu, Y.; Xia, Y. *Nanoscale* **2010**, *2*, 2406.
- (56) Jin, M.; Zhang, H.; Wang, J.; Zhong, X.; Lu, N.; Li, Z.; Xie, Z.; Kim, M. J.; Xia, Y. *ACS Nano* **2012**, *6*, 2566.
- (57) Sneed, B. T.; Young, A. P.; Jalalpoor, D.; Golden, M. C.; Mao, S.; Jiang, Y.; Wang, Y.; Tsung, C.-K. *ACS Nano* **2014**, *8*, 7239.
- (58) Kuo, C.-H.; Tang, Y.; Chou, L.-Y.; Sneed, B. T.; Brodsky, C. N.; Zhao, Z.; Tsung, C.-K. *J. Am. Chem. Soc.* **2012**, *134*, 14345.
- (59) Sneed, B. T.; Kuo, C.-H.; Brodsky, C. N.; Tsung, C.-K. *J. Am. Chem. Soc.* **2012**, *134*, 18417.
- (60) Chang, C.-C.; Wu, H.-L.; Kuo, C.-H.; Huang, M. H. *Chem. Mater.* **2008**, *20*, 7570.
- (61) Wu, H.-L.; Kuo, C.-H.; Huang, M. H. *Langmuir* **2010**, *26*, 12307.
- (62) Niu, W.; Zhang, L.; Xu, G. *ACS Nano* **2010**, *4*, 1987.
- (63) Alayoglu, S.; Nilekar, A. U.; Mavrikakis, M.; Eichhorn, B. *Nature Materials* **2008**, *7*, 333.
- (64) Grzelczak, M.; Pérez-Juste, J.; Rodríguez-González, B.; Spasova, M.; Barsukov, I.; Farle, M.; Liz-Marzán, L. M. *Chem. Mater.* **2008**, *20*, 5399.
- (65) Ping, H.; Chen, Y.; Guo, H.; Wang, Z.; Zeng, D.; Wang, L.; Peng, D.-L. *Mater. Lett.* **2014**, *116*, 239.
- (66) Stamenkovic, V. R.; Mun, B. S.; Arenz, M.; Mayrhofer, K. J. J.; Lucas, C. A.; Wang, G.; Ross, P. N.; Markovic, N. M. *Nat. Mater.* **2007**, *6*, 241.
- (67) Singh, A. K.; Xu, Q. *ChemCatChem* **2013**, *5*, 652.
- (68) Yu, W.; Porosoff, M. D.; Chen, J. G. *Chem. Rev. (Washington, DC, U. S.)* **2012**, *112*, 5780.
- (69) Debe, M. K. *Nature* **2012**, *486*, 43.
- (70) Ferrando, R.; Jellinek, J.; Johnston, R. L. *Chem. Rev. (Washington, DC, U. S.)* **2008**, *108*, 845.
- (71) Wang, D.; Li, Y. *Adv. Mater. (Weinheim, Ger.)* **2011**, *23*, 1044.
- (72) Wang, D.; Xin, H. L.; Hovden, R.; Wang, H.; Yu, Y.; Muller, D. A.; DiSalvo, F. J.; Abruña, H. D. *Nat. Mater.* **2013**, *12*, 81.
- (73) Cui, C.; Gan, L.; Li, H.-H.; Yu, S.-H.; Heggen, M.; Strasser, P. *Nano Lett.* **2012**, *12*, 5885.
- (74) Wu, Y.; Cai, S.; Wang, D.; He, W.; Li, Y. *J. Am. Chem. Soc.* **2012**, *134*, 8975.
- (75) Choi, S.-I.; Xie, S.; Shao, M.; Odell, J. H.; Lu, N.; Peng, H.-C.; Protsailo, L.; Guerrero, S.; Park, J.; Xia, X.; Wang, J.; Kim, M. J.; Xia, Y. *Nano Lett.* **2013**, *13*, 3420.
- (76) Cui, C.; Ahmadi, M.; Behafarid, F.; Gan, L.; Neumann, M.; Heggen, M.; Cuenya, B. R.; Strasser, P. *Faraday Discuss.* **2013**, *162*, 91.
- (77) Cui, C.; Gan, L.; Neumann, M.; Heggen, M.; Roldan Cuenya, B.; Strasser, P. *Journal of the American Chemical Society* **2014**, *136*, 4813.
- (78) Leonardi, A.; Leoni, M.; Siboni, S.; Scardi, P. *J. Appl. Crystallogr.* **2012**, *45*, 1162.
- (79) Kwon, K.; Lee, K. Y.; Lee, Y. W.; Kim, M.; Heo, J.; Ahn, S. J.; Han, S. W. *The Journal of Physical Chemistry C* **2007**, *111*, 1161.
- (80) Zhang, Q.; Xie, J.; Yang, J.; Lee, J. Y. *ACS Nano* **2009**, *3*, 139.
- (81) Lim, B.; Xiong, Y.; Xia, Y. *Angew. Chem.* **2007**, *119*, 9439.
- (82) Seo, D.; Yoo, C. I.; Chung, I. S.; Park, S. M.; Ryu, S.; Song, H. *The Journal of Physical Chemistry C* **2008**, *112*, 2469.
- (83) Xiong, Y.; McLellan, J. M.; Yin, Y.; Xia, Y. *Angew. Chem.* **2007**, *119*, 804.
- (84) Ling, T.; Xie, L.; Zhu, J.; Yu, H.; Ye, H.; Yu, R.; Cheng, Z.; Liu, L.; Yang, G.; Cheng, Z.; Wang, Y.; Ma, X. *Nano Lett.* **2009**, *9*, 1572.
- (85) Langille, M. R.; Zhang, J.; Personick, M. L.; Li, S.; Mirkin, C. A. *Science* **2012**, *337*, 954.
- (86) Xu, J.; Li, S.; Weng, J.; Wang, X.; Zhou, Z.; Yang, K.; Liu, M.; Chen, X.; Cui, Q.; Cao, M.; Zhang, Q. *Adv. Funct. Mater.* **2008**, *18*, 277.
- (87) Wang, Y.; Peng, H.-C.; Liu, J.; Huang, C. Z.; Xia, Y. *Nano Lett.* **2015**, *15*, 1445.
- (88) Wu, J.; Qi, L.; You, H.; Gross, A.; Li, J.; Yang, H. *Journal of the American Chemical Society* **2012**, *134*, 11880.
- (89) Lv, T.; Wang, Y.; Choi, S.-I.; Chi, M.; Tao, J.; Pan, L.; Huang, C. Z.; Zhu, Y.; Xia, Y. *ChemSusChem* **2013**, *6*, 1923.
- (90) Kang, S. W.; Lee, Y. W.; Park, Y.; Choi, B.-S.; Hong, J. W.; Park, K.-H.; Han, S. W. *ACS Nano* **2013**, *7*, 7945.
- (91) Guo, S.; Zhang, X.; Zhu, W.; He, K.; Su, D.; Mendoza-Garcia, A.; Ho, S. F.; Lu, G.; Sun, S. *J. Am. Chem. Soc.* **2014**, *136*, 15026.
- (92) Wang, C.; van der Vliet, D.; More, K. L.; Zaluzec, N. J.; Peng, S.; Sun, S.; Daimon, H.; Wang, G.; Greeley, J.; Pearson, J.; Paulikas, A. P.; Karapetrov, G.; Strmcnik, D.; Markovic, N. M.; Stamenkovic, V. R. *Nano Letters* **2011**, *11*, 919.
- (93) Choi, S.-I.; Shao, M.; Lu, N.; Ruditskiy, A.; Peng, H.-C.; Park, J.; Guerrero, S.; Wang, J.; Kim, M. J.; Xia, Y. *ACS Nano* **2014**, *8*, 10363.
- (94) Kuttiyil, K. A.; Sasaki, K.; Su, D.; Vukmirovic, M. B.; Marinkovic, N. S.; Adzic, R. R. *Electrochim. Acta* **2013**, *110*, 267.
- (95) Kang, Y.; Snyder, J.; Chi, M.; Li, D.; More, K. L.; Markovic, N. M.; Stamenkovic, V. R. *Nano Lett.* **2014**, *14*, 6361.
- (96) Ferrer, D.; Torres-Castro, A.; Gao, X.; Sepúlveda-Guzmán, S.; Ortiz-Méndez, U.; José-Yacamán, M. *Nano Lett.* **2007**, *7*, 1701.
- (97) Zhang, H.; Jin, M.; Wang, J.; Kim, M. J.; Yang, D.; Xia, Y. *J. Am. Chem. Soc.* **2011**, *133*, 10422.
- (98) Qiu, F.; Liu, G.; Li, L.; Wang, Y.; Xu, C.; An, C.; Chen, C.; Xu, Y.; Huang, Y.; Wang, Y.; Jiao, L.; Yuan, H. *Chemistry – A European Journal* **2014**, *20*, 505.
- (99) Aranishi, K.; Jiang, H.-L.; Akita, T.; Haruta, M.; Xu, Q. *Nano Research* **2011**, *4*, 1233.
- (100) Xin, H. L.; Mundy, J. A.; Liu, Z.; Cabezas, R.; Hovden, R.; Kourkoutis, L. F.; Zhang, J.; Subramanian, N. P.; Makharia, R.; Wagner, F. T.; Muller, D. A. *Nano Letters* **2012**, *12*, 490.
- (101) Petkov, V.; Wanjala, B. N.; Loukrakpam, R.; Luo, J.; Yang, L.; Zhong, C.-J.; Shastri, S. *Nano Lett.* **2012**, *12*, 4289.

- (102) Scardi, P.; Leonardi, A.; Gelisio, L.; Suchomel, M. R.; Sneed, B. T.; Sheehan, M. K.; Tsung, C. K. *Physical Review B* **2015**, *91*, 155414.
- (103) Gordon, T. R.; Diroll, B. T.; Paik, T.; Doan-Nguyen, V. V. T.; Gaudling, E. A.; Murray, C. B. *Chem. Mater.* **2015**.
- (104) Robinson, I.; Harder, R. *Nat. Mater.* **2009**, *8*, 291.
- (105) Sau, T. K.; Rogach, A. L. *Advanced Materials (Weinheim, Germany)* **2010**, *22*, 1781.
- (106) Chen, M.; Wu, B.; Yang, J.; Zheng, N. *Advanced Materials (Weinheim, Germany)* **2012**, *24*, 862.
- (107) Peng, H.-C.; Xie, S.; Park, J.; Xia, X.; Xia, Y. *Journal of the American Chemical Society* **2013**, *135*, 3780.
- (108) Xie, S.; Zhang, H.; Lu, N.; Jin, M.; Wang, J.; Kim, M. J.; Xie, Z.; Xia, Y. *Nano Lett.* **2013**, *13*, 6262.
- (109) Zheng, Y.; Luo, M.; Tao, J.; Peng, H.-C.; Wan, D.; Zhu, Y.; Xia, Y. *The Journal of Physical Chemistry B* **2014**, *118*, 14132.
- (110) Long, R.; Zhou, S.; Wiley, B. J.; Xiong, Y. *Chem. Soc. Rev.* **2014**, *43*, 6288.
- (111) Zhang, J.; Feng, C.; Deng, Y.; Liu, L.; Wu, Y.; Shen, B.; Zhong, C.; Hu, W. *Chem. Mater.* **2014**, *26*, 1213.
- (112) Dai, Y.; Mu, X.; Tan, Y.; Lin, K.; Yang, Z.; Zheng, N.; Fu, G. *J. Am. Chem. Soc.* **2012**, *134*, 7073.
- (113) Ma, L.; Wang, C.; Xia, B. Y.; Mao, K.; He, J.; Wu, X.; Xiong, Y.; Lou, X. W. *Angewandte Chemie International Edition* **2015**, n/a.
- (114) Wu, J.; Gross, A.; Yang, H. *Nano Lett.* **2011**, *11*, 798.
- (115) Kang, Y.; Pyo, J. B.; Ye, X.; Diaz, R. E.; Gordon, T. R.; Stach, E. A.; Murray, C. B. *ACS Nano* **2013**, *7*, 645.
- (116) Bhattarai, N.; Casillas, G.; Khanal, S.; Salazar, J. J.; Ponce, A.; Jose-Yacamán, M. *Journal of Nanoparticle Research* **2013**, *15*, 1.
- (117) Deng, Y.-J.; Tian, N.; Zhou, Z.-Y.; Huang, R.; Liu, Z.-L.; Xiao, J.; Sun, S.-G. *Chemical Science* **2012**, *3*, 1157.
- (118) Zhang, J.; Zhang, L.; Xie, S.; Kuang, Q.; Han, X.; Xie, Z.; Zheng, L. *Chemistry – A European Journal* **2011**, *17*, 9915.
- (119) Tian, N.; Zhou, Z.-Y.; Sun, S.-G. *The Journal of Physical Chemistry C* **2008**, *112*, 19801.
- (120) Tran, T. T.; Lu, X. *The Journal of Physical Chemistry C* **2011**, *115*, 3638.
- (121) Huang, X.; Zhao, Z.; Fan, J.; Tan, Y.; Zheng, N. *J. Am. Chem. Soc.* **2011**, *133*, 4718.
- (122) Wang, L.-B.; Wang, Y.-C.; Guo, H.-Y.; Huang, J.-L.; Zhao, Y.-L.; Liu, Q.-Y.; Wu, X.; Zeng, J. *Particle & Particle Systems Characterization* **2014**, n/a.
- (123) Wang, L.-B.; Wang, Y.-C.; Guo, H.-Y.; Huang, J.-L.; Zhao, Y.-L.; Liu, Q.-Y.; Wu, X.; Zeng, J. *Particle & Particle Systems Characterization* **2015**, *32*, 295.
- (124) Tian, N.; Zhou, Z.-Y.; Sun, S.-G.; Ding, Y.; Wang, Z. L. *Science* **2007**, *316*, 732.
- (125) Jia, Y.; Jiang, Y.; Zhang, J.; Zhang, L.; Chen, Q.; Xie, Z.; Zheng, L. *Journal of the American Chemical Society* **2014**, *136*, 3748.
- (126) Chen, C.; Kang, Y.; Huo, Z.; Zhu, Z.; Huang, W.; Xin, H. L.; Snyder, J. D.; Li, D.; Herron, J. A.; Mavrikakis, M.; Chi, M.; More, K. L.; Li, Y.; Markovic, N. M.; Somorjai, G. A.; Yang, P.; Stamenkovic, V. R. *Science* **2014**, *343*, 1339.
- (127) Zhang, C.; Sandorf, W.; Peng, Z. *ACS Catalysis* **2015**, 2296.
- (128) Stepanyuk, V. S.; Bazhanov, D. I.; Baranov, A. N.; Hergert, W.; Dederichs, P. H.; Kirschner, J. *Physical Review B* **2000**, *62*, 15398.
- (129) Xie, S.; Choi, S.-I.; Lu, N.; Roling, L. T.; Herron, J. A.; Zhang, L.; Park, J.; Wang, J.; Kim, M. J.; Xie, Z.; Mavrikakis, M.; Xia, Y. *Nano Lett.* **2014**, *14*, 3570.
- (130) Lu, N.; Wang, J.; Xie, S.; Brink, J.; McIlwrath, K.; Xia, Y.; Kim, M. J. *The Journal of Physical Chemistry C* **2014**, *118*, 28876.
- (131) Park, J.; Zhang, L.; Choi, S.-I.; Roling, L. T.; Lu, N.; Herron, J. A.; Xie, S.; Wang, J.; Kim, M. J.; Mavrikakis, M.; Xia, Y. *ACS Nano* **2015**.
- (132) Lim, G.-H.; Yu, T.; Koh, T.; Lee, J. H.; Jeong, U.; Lim, B. *Chem. Phys. Lett.* **2014**, *595–596*, 77.
- (133) Zheng, L.; Xiong, L.; Sun, J.; Li, J.; Yang, S.; Xia, J. *Catal. Commun.* **2008**, *9*, 624.
- (134) Zhao, Y.; Kornienko, N.; Liu, Z.; Zhu, C.; Asahina, S.; Kuo, T.-R.; Bao, W.; Xie, C.; Hexemer, A.; Terasaki, O.; Yang, P.; Yaghi, O. M. *J. Am. Chem. Soc.* **2015**, *137*, 2199.
- (135) Snyder, J.; Fujita, T.; Chen, M. W.; Erlebacher, J. *Nat. Mater.* **2010**, *9*, 904.
- (136) Snyder, J.; Livi, K.; Erlebacher, J. *Advanced Functional Materials* **2013**, *23*, 5494.
- (137) Holton, O. T.; Stevenson, J. W. *Platinum Metals Review* **2013**, *57*, 259.
- (138) Cui, C.; Gan, L.; Heggen, M.; Rudi, S.; Strasser, P. *Nat. Mater.* **2013**, *12*, 765.
- (139) Menning, C. A.; Chen, J. G. *The Journal of Chemical Physics* **2009**, *130*, 174709.
- (140) Wang, G.; Van Hove, M. A.; Ross, P. N.; Baskes, M. I. *The Journal of Chemical Physics* **2005**, 122.
- (141) Ruban, A. V.; Skriver, H. L.; Nørskov, J. K. *Physical Review B* **1999**, *59*, 15990.
- (142) Wang, L.-L.; Johnson, D. D. *J. Am. Chem. Soc.* **2009**, *131*, 14023.
- (143) Turchanin, M. A.; Agraval, P. G. *Powder Metallurgy and Metal Ceramics* **2008**, *47*, 26.
- (144) Vitos, L.; Ruban, A. V.; Skriver, H. L.; Kollár, J. *Surf. Sci.* **1998**, *411*, 186.
- (145) Tao, F.; Grass, M. E.; Zhang, Y.; Butcher, D. R.; Aksoy, F.; Aloni, S.; Altoe, V.; Alayoglu, S.; Renzas, J. R.; Tsung, C.-K.; Zhu, Z.; Liu, Z.; Salmeron, M.; Somorjai, G. A. *J. Am. Chem. Soc.* **2010**, *132*, 8697.
- (146) Tao, F.; Grass, M. E.; Zhang, Y.; Butcher, D. R.; Renzas, J. R.; Liu, Z.; Chung, J. Y.; Mun, B. S.; Salmeron, M.; Somorjai, G. A. *Science* **2008**, *322*, 932.
- (147) Gan, L.; Heggen, M.; O'Malley, R.; Theobald, B.; Strasser, P. *Nano Letters* **2013**, *13*, 1131.
- (148) Gan, L.; Cui, C.; Heggen, M.; Dionigi, F.; Rudi, S.; Strasser, P. *Science* **2014**, *346*, 1502.
- (149) Brodsky, C. N.; Young, A. P.; Ng, K. C.; Kuo, C.-H.; Tsung, C.-K. *ACS Nano* **2014**, *8*, 9368.
- (150) Cheng, J.; Hu, P. *Journal of the American Chemical Society* **2008**, *130*, 10868.
- (151) Bhattarai, N.; Casillas, G.; Ponce, A.; Jose-Yacamán, M. *Surf. Sci.* **2013**, *609*, 161.
- (152) Wang, L.; Liu, P.; Guan, P.; Yang, M.; Sun, J.; Cheng, Y.; Hirata, A.; Zhang, Z.; Ma, E.; Chen, M.; Han, X. *Nat Commun* **2013**, *4*.
- (153) Kwon, S. G.; Krylova, G.; Phillips, P. J.; Klie, R. F.; Chattopadhyay, S.; Shibata, T.; Bunel, E. E.; Liu, Y.; Prakapenka, V. B.; Lee, B.; Shevchenko, E. V. *Nature Materials* **2015**, *14*, 215.
- (154) Zheng, H.; Cao, A.; Weinberger, C. R.; Huang, J. Y.; Du, K.; Wang, J.; Ma, Y.; Xia, Y.; Mao, S. X. *Nat Commun* **2010**, *1*, 144.
- (155) Gutkin, M. Y.; Smirnov, A. M. *Acta Mater.* **2015**, *88*, 91.
- (156) Gutkin, M. Y.; Kolesnikova, A. L.; Krasnitckii, S. A.; Romanov, A. E.; Shalkovskii, A. G. *Scr. Mater.* **2014**, *83*, 1.

TOC GRAPHIC

